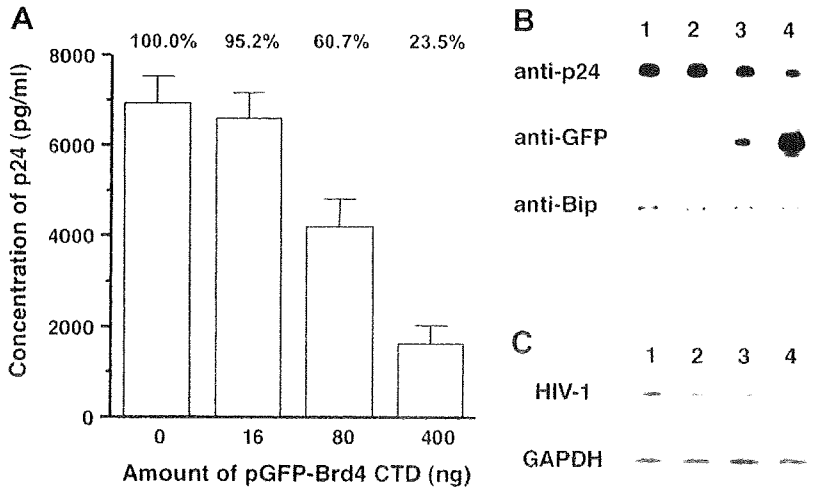

Fig. 2. Inhibition of HIV-1 production by GFP-Brd4-CTD. (A) Viral production was quantified by ELISA detecting p24 viral antigen. The relative decrease in viral levels are indicated on the top of the graph. (B) The viral protein levels in transfected cells were analyzed by Western blotting using the antibodies indicated. (C) The viral spliced transcript and GAPDH mRNA were amplified by RT-PCR. Lanes 1–4 in B and C correspond to the amount of pGFP-Brd4-CTD (0, 16, 80, and 400 ng, respectively). Quantification of these data is summarized in Table 2.

activity was markedly enhanced. When the GFP-Brd4-CTD expression vector was co-transfected, the Tat-dependent enhancement of LTR promoter-driven luciferase expression decreased. A similar trend was not observed for the CMV promoter. These data suggest that the Brd4-CTD specifically limits Tat-dependent LTR transcription.

We also investigated the effect of GFP-Brd4-CTD expression on HIV-1 production by using a proviral DNA mimicking the late phase of the viral life cycle. Consistent with the results described above, transfection of HIV-1 proviral DNA together with an increasing amount of the GFP-Brd4-CTD expression vector led to a decrease of viral yield, as well as of the levels of viral protein and mRNA in the transfected cells (Fig. 2). The viral RNA levels dropped in parallel with the protein levels, as demonstrated by real-time RT-PCR analysis (Fig. 2C and Table 2). These data suggest that GFP-Brd4-CTD inhibits HIV-1 production by blocking viral transcription.

To confirm the blockage of HIV-1 replication by Brd4-CTD, GFP-Brd4-CTD was transduced into MT-4 and Jurkat cells using an MLV-based vector (Fig. 3A). Green fluorescence indicated that the efficiency of MLV-mediated gene transduction in MT-4 cells was >90%, with a lower transduction efficiency observed in Jurkat cells, as estimated by FACS analysis. The GFP-positive Jurkat cells were collected using a FACS sorter. The expression of GFP and GFP-Brd4-CTD was verified by Western blot analysis (Fig. 3B). The expression levels of transcription-related gene products were not detectably affected by the constitutive expression of GFP-Brd4-CTD (Fig. 3B). In addition, there was no detectable difference in the levels of cell-surface HIV-1 receptors (CD4 and CXCR4), cell morphology, and cell proliferation rates between GFP- and GFP-Brd4-CTD-expressing cells (Fig. 1C and Supplementary data). We found that HIV-1 replicated less efficiently in GFP-Brd4-CTD-expressing cells than in GFP-expressing cells, in both cell lines tested, which confirms the HIV-1-resistant phenotype of MT-4 cells (Fig. 3C). The efficiency of viral genome integration into GFP-Brd4-CTD-expressing cells was indistinguishable from that of GFP-expressing cells (103.2 ± 24.1%) as examined by Alu-LTR PCR, suggesting that the early phase of the viral life cycle was not blocked by GFP-Brd4-CTD.

4. Discussion

Our phenotype screening method proved to be a powerful tool because a human T cell line was subjected to HIV-1 resistance screening by stable and non-transient introduction of a human cDNA library, and because wild-type HIV-1 was used; thus, the effect of candidate gene expression on cell proliferation was less of a concern in this system when compared with transient assay systems. In addition, HIV-1 inhibitory genes were isolated at a frequency of ~15% (4/26 genes), 75% of which were novel. We therefore believe that our system is remarkable in selecting genes that confer HIV-1 resistance in T cells. By applying this assay to other cDNA libraries, we

Table 2
Effect of GFP-Brd4-CTD on viral production examined by quantitative real time RT-PCR and ELISA.

pGFP-Brd4-CTD (ng)	HIV-1 mRNA (copy)[a]	GAPDH mRNA (copy)[a]	Ratio (HIV-1/GAPDH)	Normalized (%)[b]	p24 ELISA (%)[c]
0	274250	261750	1.048	100.0	100.0
16	221600	228850	0.968	92.4	95.2
80	138050	311450	0.443	42.3	60.7
400	120850	347750	0.348	33.2	23.5

[a]Copy per 100 ng total cellular RNA.
[b]Relative reduction of HIV-1 mRNA considering pGFP-Brd4-CTD 0 ng as 100%.
[c]See Fig. 2.

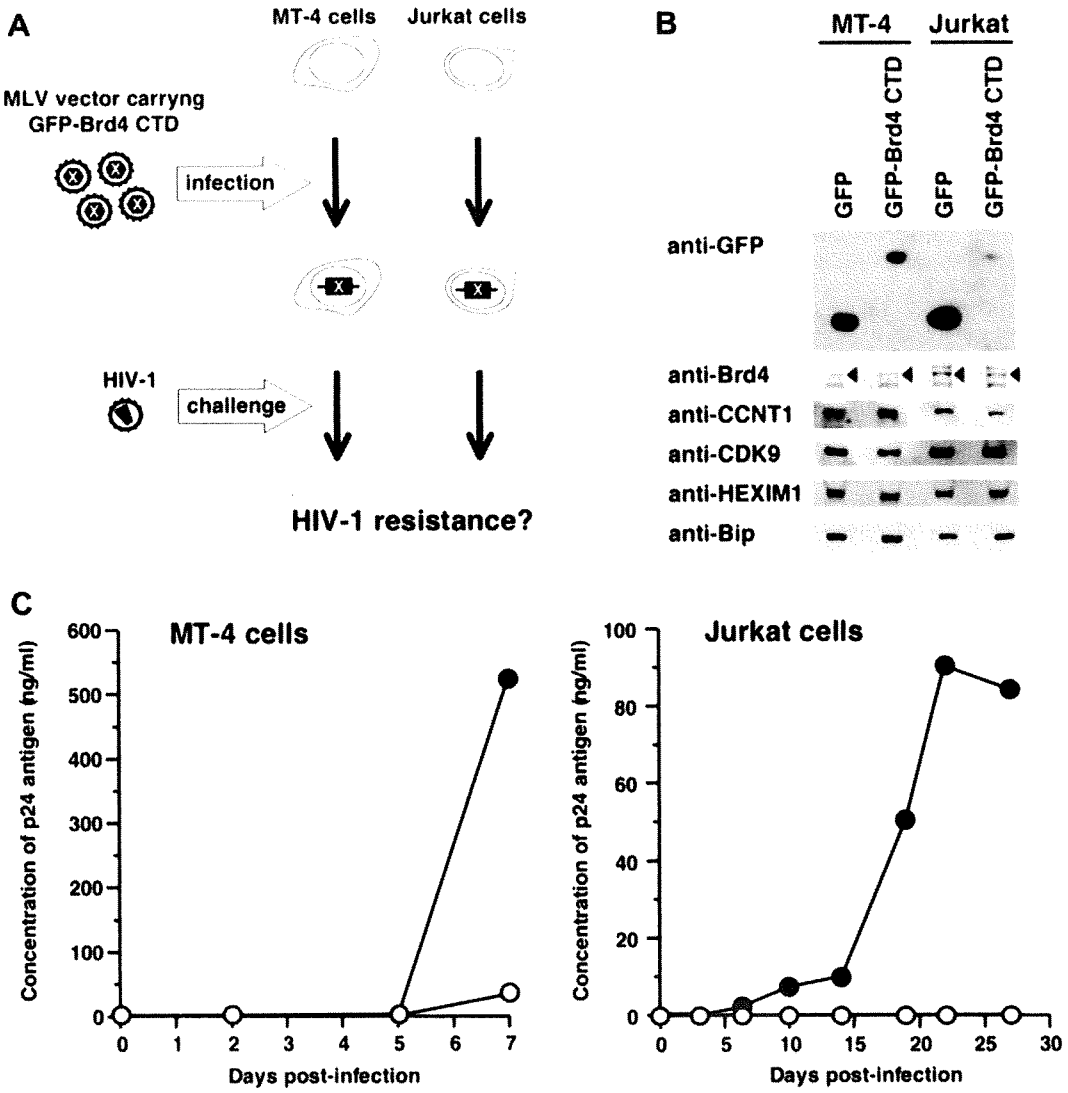

Fig. 3. Constitutive expression of GFP-Brd4-CTD limited the replication of HIV-1. (A) Experimental design. MT-4 and Jurkat cells were transduced with an MLV vector expressing GFP-Brd4-CTD. Cells were challenged by HIV-1 and the efficiency of viral replication was examined. (B) Western blot analysis of the expression levels of GFP, GFP-Brd4-CTD, Brd4 (arrowhead), CCNT1, CDK9, HEXIM1, and BiP in established MT-4 and Jurkat cells. (C) HIV-1 replication kinetics in MT-4 and Jurkat cells constitutively expressing GFP (black circles) or GFP-Brd4-CTD (white circles). Representative data from two independent experiments are shown.

may be able to isolate novel cellular factors that regulate HIV-1 replication.

The assessment of the selective impact of altered candidate gene expression or function on HIV-1 replication (without the alteration of cell proliferation) is critical to the identification of cellular molecular targets for novel anti-retroviral drugs. We demonstrated that Brd4-CTD was a specific silencer of HIV-1 replication, and verified that it effectively blocked HIV-1 replication in multiple human T cell lines without affecting cell proliferation. Our data indicate that primate lentiviral replication is more heavily dependent on the CCNT1-containing P-TEFb complex than cellular gene transcription, which is consistent with previous findings [4,10–11]. This implies that HIV-1 replication can be controlled by selectively restricting the CCNT1-containing P-TEFb complex. Our transcription assay indicated that the Brd4-CTD is not an inhibitor of the P-TEFb complex, but is rather a functional Tat inhibitor. Previous biochemical studies have suggested that Brd4-CTD and Tat bind to CCNT1 in a reciprocally exclusive fashion [7,9]. Given that the binding regions of these two proteins do not overlap, Brd4-CTD may be an allosteric inhibitor of the Tat-CCNT1 interaction. Taken together, our results indicate that the Brd4-interacting region of CCNT1 is a potential molecular target for the development of a novel HIV-1 inhibitor.

Acknowledgements: This work was supported by the Japan Health Science Foundation, the Japanese Ministry of Health, Labor and Welfare (H18-AIDS-W-003) and the Japanese Ministry of Education, Culture, Sports, Science and Technology (18689014 and 18659136).

Appendix A. Supplementary data

Supplementary data associated with this article can be found, in the online version, at doi:10.1016/j.febslet.2008.10.047.

References

[1] Valente, S.T. and Goff, S.P. (2006) Inhibition of HIV-1 gene expression by a fragment of hnRNP U. Mol. Cell 23, 597–605.

[2] Brass, A.L., Dykxhoorn, D.M., Benita, Y., Yan, N., Engelman, A., Xavier, R.J., Lieberman, J. and Elledge, S.J. (2008) Identification of host proteins required for HIV infection through a functional genomic screen. Science 319, 921–926.

[3] Komano, J., Miyauchi, K., Matsuda, Z. and Yamamoto, N. (2004) Inhibiting the Arp2/3 complex limits infection of both intracellular mature vaccinia virus and primate lentiviruses. Mol. Biol. Cell 15, 5197–5207.

[4] Shimizu, S. et al. (2007) Inhibiting lentiviral replication by HEXIM1, a cellular negative regulator of the CDK9/cyclin T complex. AIDS 21, 575–582.

[5] Kawano, Y., Yoshida, T., Hieda, K., Aoki, J., Miyoshi, H. and Koyanagi, Y. (2004) A lentiviral cDNA library employing lambda recombination used to clone an inhibitor of human immunodeficiency virus type 1-induced cell death. J. Virol. 78, 11352–11359.

[6] Biglione, S., Byers, S.A., Price, J.P., Nguyen, V.T., Bensaude, O., Price, D.H. and Maury, W. (2007) Inhibition of HIV-1 replication by P-TEFb inhibitors DRB, seliciclib and flavopiridol correlates with release of free P-TEFb from the large, inactive form of the complex. Retrovirology 4, 47.

[7] Jang, M., Mochizuki, K., Zhou, M., Jeong, H., Brady, J. and Ozato, K. (2005) The bromodomain protein Brd4 is a positive regulatory component of P-TEFb and stimulates RNA polymerase II-dependent transcription. Mol. Cell 19, 523–534.

[8] Yang, Z., Yik, J., Chen, R., He, N., Jang, M., Ozato, K. and Zhou, Q. (2005) Recruitment of P-TEFb for stimulation of transcriptional elongation by the bromodomain protein Brd4. Mol. Cell 19, 535–545.

[9] Bisgrove, D.A., Mahmoudi, T., Henklein, P. and Verdin, E. (2007) Conserved P-TEFb-interacting domain of BRD4 inhibits HIV transcription. Proc. Natl. Acad. Sci. USA 104, 13690–13695.

[10] Urano, E. et al. (2008) Cyclin K/CPR4 inhibits primate lentiviral replication by inactivating Tat/positive transcription elongation factor b-dependent long terminal repeat transcription. AIDS 22, 1081–1083.

[11] Salerno, D., Hasham, M.G., Marshall, R., Garriga, J., Tsygankov, A.Y. and Grana, X. (2007) Direct inhibition of CDK9 blocks HIV-1 replication without preventing T-cell activation in primary human peripheral blood lymphocytes. Gene 405, 65–78.

ELSEVIER

INSTITUT PASTEUR

Microbes and Infection 10 (2008) 1514–1523

www.elsevier.com/locate/micinf

Original article

Primary target cells of herpes simplex virus type 1 in the hippocampus

Yoshinori Ando [a,b], Hiroko Kitayama [a], Yasushi Kawaguchi [c], Yoshio Koyanagi [a,*]

[a] *Laboratory of Viral Pathogenesis, Institute for Virus Research, Kyoto University, 53 Shogoin-kawara-cho, Sakyo-ku, Kyoto 606-8507, Japan*
[b] *Department of Molecular and Cellular Biology, Graduate School of Biostudies, Kyoto University, Yoshida-konoe-cho, Sakyo-ku, Kyoto 606-8501, Japan*
[c] *Division of Viral Infection, Department of Infectious Disease Control, International Research Center for Infectious Diseases, The Institute of Medical Science, The University of Tokyo, 4-6-1 Shirokanedai, Minato-ku, Tokyo 108-8639, Japan*

Received 24 April 2008; accepted 3 September 2008
Available online 25 September 2008

Abstract

Herpes simplex virus type 1 (HSV-1) causes fatal and sporadic encephalitis in human. The encephalitis-survivors frequently suffer from symptoms of memory deficits. It remains unclear how HSV-1 induces tissue damages in memory formation-associated brain tissues such as the hippocampus. In this study, we examined HSV-1 infection in the hippocampus using a rat HSV-1 infection model. We found profound pathological changes in the hippocampus and large numbers of HSV-1 antigen-positive cells in the dentate gyrus (DG) subfield of HSV-1-infected rats. To understand the precise mechanism of HSV-1-induced tissue damages in the hippocampus, we employed rat organotypic hippocampal slice cultures (OHC) as an in vitro HSV-1 infection model. In OHC, HSV-1 infection predominated in neuronal cells and the infected neuronal cells were severely damaged. Longitudinal analysis indicated that granule cells in DG subfield were extremely vulnerable to HSV-1 infection among neuronal cells in the hippocampus. Since DG granule cells play a crucial role in memory formation, disruption of these cells may be a primary step leading to memory deficits.

Keywords: HSV-1; Hippocampus; Organotypic hippocampal slice cultures; Dentate gyrus; Neuron

1. Introduction

Herpes simplex virus (HSV) frequently invades the central nervous system (CNS) and induces severe encephalitis (HSV encephalitis, HSE) in human. HSE patients show several symptoms including fever, headache, mental abnormalities, seizure, and aphasia [1–5]. HSE survivors often suffer from neurological sequelae, most frequently, memory deficit [6]. Typical pathological changes in HSE are necrotization in medial temporal lobe and orbital surface of frontal lobe [5]. The amnestic impairments have been explained by the damages in medial temporal lobe [6]. Temporal lobe contains the limbic systems, including the hippocampus, the amygdala, the entorhinal and perirhinal cortex, that are critical for declarative anterograde memory [6]. It has been reported that HSV-1 antigen-positive cells are frequently found in these limbic regions of HSE patients [1,3,7].

The hippocampus tissue is highly vulnerable to anoxia, ischemia, and tissue damages caused by viruses such as human immunodeficiency virus 1 (HIV-1), borna disease virus (BDV), and HSV. In HIV-infected models, the hippocampus is damaged likely by viral and host factors released from HIV-1-infected macrophages [8,9]. In BDV-infected rats, selective neuronal cell degeneration occurs in the dentate gyrus (DG) [10].

In the present study, we examined the mechanism of HSV-1 infection in the hippocampus. Using organotypic hippocampal slice cultures (OHC), we found that HSV-1 primarily attacked neuronal cells but not glial cells. More importantly, among neuronal cells in the hippocampus, we found that granule cells in DG subfield were initially killed through HSV-1-mediated cytopathic effect, suggesting that DG granule cells were primary HSV-1 victims in the hippocampus.

* Corresponding author. Tel.: +81 75 751 4811; fax: +81 75 751 4812.
E-mail address: ykoyanag@virus.kyoto-u.ac.jp (Y. Koyanagi).

1286-4579/$ - see front matter © 2008 Elsevier Masson SAS. All rights reserved.
doi:10.1016/j.micinf.2008.09.005

2. Materials and methods

2.1. Cells and viruses

Vero cell line was maintained in Dulbecco's modified Eagle Medium supplemented with 10% fetal calf serum. A wild-type HSV-1, HSV-1 strain F [HSV-1 (F)] and a green fluorescent protein (GFP)-expressing replication-competent HSV-1 (YK333) [11], which is HSV-1 (F)-based and replicates in a similar manner with HSV-1 (F) in Vero cells, were propagated in Vero cells and the titers were determined by standard 50% tissue culture infective dose ($TCID_{50}$) on Vero cells.

2.2. HSV-1 infection in rats and tissue collection

Fourteen-day-old Wistar Hannover GALAS rats (CLEA Japan, Inc., Japan) were intranasally inoculated with 5×10^5 $TCID_{50}$ HSV-1 (F) or phosphate-buffered saline (PBS) [12]. When inoculated rats showed weakening with weight loss, trembling, paralysis, and/or seizure, the animals were sacrificed and brain tissues were collected. For histological examinations, samples were fixed by immersion in 4% paraformaldehyde, and then sectioned using a cryostat microtome and were stained with hematoxylin and eosin (HE). The degree of tissue damages in brain tissues was classified into 4 groups and the percentage of the area displaying cell lost in the coronal section was shown as follows: −, <5%; +, 5–10%; ++, 10–30%; +++, >30%. To estimate neuronal cell loss in brain tissues, neuronal nuclei (NeuN) were immunostained and the intensity was quantified using Image J software. Data were normalized with that in PBS-inoculated rat. The degree of neuronal cell loss was shown as NeuN intensity ratio and was classified into 4 groups: +++, <0.3; ++, 0.3–0.5; +, 0.5–0.9; −, >0.9. All animal experiments were carried out according to the guidelines for animal experimentation at the Kyoto University.

2.3. Organotypic hippocampal slice cultures and HSV-1 infection

OHC were prepared from postnatal day 7–8 Wistar Hannover GALAS rats (CLEA Japan, Inc.) as previously described [9,13]. Two weeks after initiation of culture, slice cultures were cocultured with HSV-1-infected Vero cells. The Vero cells were infected on the previous day at multiplicity of infection of 1. Twelve hours after cocultivation, the slices were transferred to fresh medium and cultured. HSV-1 titers in the slices were measured by standard $TCID_{50}$ method after the slices were homogenized. For inhibition of HSV-1, we added 25 μg/ml of acyclovir (Sigma-Aldrich, St. Louis, MO, USA) in culture medium.

2.4. PCR

Polymerase chain reaction (PCR) was carried out using AmpliTaq Gold (Applied Biosystems Japan, Ltd., Japan) according to the manufacturer's protocol. One hundred nanogram of sample DNA was used. PCR product of HSV-1 glycoprotein B (gB) and glyceraldehyde-3-phosphate dehydrogenase (GAPDH) were obtained after amplification for 35 and 30 cycles, respectively. Specific primer pairs against HSV-1 gB and GAPDH are as follows: gB-F, 5′-TCGCCTTTCGCTACGTCAT-3′; gB-R, 5′-GGTTCTTGA GCTCCTTGGTGG-3′; GAPDH-F, 5′-ACTAAAGGGCATC CTGGGCTA-3′; GAPDH-R, 5′-TGGAAGAATGGGAGTTG CTGT-3′.

2.5. Antibodies

The following antibodies were used: anti-HSV and anti-glial fibrillary acidic protein (GFAP) rabbit polyclonal antibodies (DakoCytomation, Carpinteria, CA, USA); anti-HSV-1 ICP27 and anti-HSV-1 gB goat polyclonal antibodies (Santa Cruz Biotechnology, Inc., Santa Cruz, CA, USA); anti-HSV-1 ICP5 mouse monoclonal antibody (clone 3B6, Virusys Corporation, Sykesville, MD, USA); anti-NeuN mouse monoclonal antibody (clone A60, Chemicon International, Inc., Temecula, CA, USA); Alexa Fluor 488-conjugated goat anti-mouse and Alexa Fluor 594-conjugated goat anti-rabbit IgG (Invitrogen, Carlsbad, CA, USA); fluorescein isothiocyanate (FITC)-conjugated donkey anti-goat IgG (Chemicon International, Inc.).

2.6. Immunohistochemistry

Rat brain sections were permeabilized with 0.1% Triton X-100, then were incubated with blocking buffer containing 5% normal goat serum (Vector Laboratories, Inc., Burlingame, CA, USA), followed by incubation with primary antibodies. Samples were subsequently incubated with secondary antibodies. Immunohistochemical (IHC) staining and examination of OHC were carried out as previously described [9]. Nuclei were stained using Hoechst33342 dye (Invitrogen).

2.7. Measurement of cell damage in OHC

Cellular uptake of propidium iodide (PI, Invitrogen) was used for the estimation of cell damage [14]. PI was added at 5 μg/ml and the cultures were incubated for 30 min at 34 °C. Nuclei were stained using Hoechst33342 dye (Invitrogen). Each sample was examined under a confocal laser microscope (TCS SP2 AOBS, Leica Microsystems, Heidelberg, Germany). The quantification of fluorescent intensity was done following the protocol supplied by manufacturer (LCS Lite software, Leica Microsystems).

2.8. Statistical analysis

Data were generated from at least three replicate experiments. Statistical analysis was carried out by one-way ANOVA. Multiple comparisons were performed with Student's t test. A P value of less than 0.05 was considered significant.

3. Results

3.1. HSV-1 induces neuronal cell loss in the hippocampus

We first studied the pathogenesis of HSE in rats intranasally inoculated with HSV-1 (F). A total of 9 rats were infected, and within 3 days post infection (dpi), all rats appeared healthy. However, among them, 8 rats (#1–8) showed severe weakening with weight loss, trembling, and the symptoms of severe encephalitis such as paralysis and/or seizures on 4 or 5 dpi. Although one rat of the infected group (#9) gained weight and had no neurological illness similar to PBS-inoculated rat prior to 7 dpi, after 7 dpi, body weight gradually decreased and it showed weakening with trembling and paralysis (Fig. 1A). We confirmed HSV-1 infection by PCR analysis using HSV-1 gB-specific primers. Tissue damages were evaluated by histological examination in brain tissues, although tissue samples from some of the infected rats (#4, #6, and #8) were not available because of sudden deaths by severe encephalitis. As shown in Fig. 1B, HSV-1 gB DNA was detected by 4 dpi in the cerebral cortex, the hippocampus, the olfactory bulb, and the trigeminal ganglia of the infected rats but not in those of mock-infected (PBS-inoculated) rat (Fig. 1B). HE-stained brain sections from 4 to 10 dpi revealed tissue damages displaying focal hemorrhagic cell loss and cell infiltration in cerebral cortex, the hippocampus, and the medulla of the infected rats (Fig. 1C and Table 1). These data indicate that HSV-1 efficiently disseminates to the hippocampus as well as other brain tissues and induces hippocampal damages. Since it is well known that the hippocampus forms neuronal network and that this is essential for memory formation [15], we next examined neuronal cell loss in the hippocampus. Co-immunostaining for NeuN and HSV-1 in brain sections from 4 to 10 dpi indicated that the number of NeuN antigen-positive neuronal cells in the hippocampus of HSV-1-infected rats was severely reduced as similar to other regions of brain such as cerebral cortex and medulla (Fig. 1D a, b and Table 1), and large numbers of HSV-1 antigen-positive cells were found in the hippocampus (Fig. 1D a and c). Notably, many of HSV-1 antigen-positive cells were localized at DG subfield, suggesting that DG granule cells might be preferentially infected with HSV-1. Large numbers of HSV-1 antigen-positive cells were also found in other regions of brain (data not shown). These data indicate that HSV-1 infection induces severe neuronal cell loss at the hippocampus.

3.2. Longitudinal analysis of HSV-1 infection in the CNS using organotypic hippocampal slice cultures

Since animal models have limitations for longitudinal pathological analyses, we employed OHC. Physiological and morphological features of OHC closely resemble those of the actual hippocampus and would provide an alternative model to the hippocampus in vivo. As cellular composition and architecture within the hippocampus are well preserved in OHC, the main neuronal network organization is very similar to that of living animals [9,16]. However, unlike the bona fide hippocampus, in OHC, there are layers of glial cells above and below the main area containing neuronal cell layers [13]. For this reason, the slices were exposed to HSV-1 released from the infected Vero cells across the porous membrane to efficiently infect the neuronal cells and the glial cells that are immersed in slice cultures with HSV-1. To examine the precise mechanism of HSV-1-induced hippocampal damages in vitro, we first verified the longitudinal alteration of OHC by HSV-1 infection. We measured virus titers in the slices. As shown in Fig. 2A, the highest level of virus production was detected on 5 dpi and virus production was maintained for at least 10 days. After the slices were infected with HSV-1 (F), neuronal cell layers were gradually destroyed and their tissue architectures were largely disrupted by 10 dpi (Fig. 2B, top panels). To visualize longitudinal HSV-1 dissemination, we next used a GFP-expressing replication-competent HSV-1, HSV-1 (YK333). We confirmed that similar level of HSV-1 production took place in HSV-1 (YK333)-infected slices compared to that in HSV-1 (F)-infected slices (Fig. 2A). GFP-positive cells were initially detected in the borders of the slices at 3 dpi. Keeping with cultivation, HSV-1 (YK333) massively disseminated to entire slices by 5 dpi and then GFP expression was gradually reduced. In accordance with this, the tissue architectures of HSV-1 (YK333)-infected slices were gradually disrupted as were in HSV-1 (F)-infected slices (Fig. 2B, middle panels). In addition, we tested whether an anti-HSV drug, acyclovir, exhibited the capacity to inhibit HSV-1 replication in OHC. As shown to Fig. 2C, addition of acyclovir to the culture medium starting at 24 h prior to HSV-1 (YK333) infection remarkably inhibited HSV-1 dissemination in the slices, and their tissue architectures were also not affected (Fig. 2C, top panels). However, when acyclovir treatment was started on 3 dpi, HSV-1 could disseminate to entire slices and the tissue architectures of the slices were gradually destroyed as a similar manner to untreated slices (Fig. 2C, bottom panels). We also examined and confirmed with HSV-1 (F) (data not shown). From these longitudinal analyses, HSV-1 infection may have occurred in the neuronal cells and the glial cells on 5 dpi. To confirm this, viral proteins in HSV-1 (F)-infected slices were immunostained. In the infected slices on 1 and 3 dpi, viral proteins were expressed only in a part of the slices as similar to the results obtained using HSV-1 (YK333) (data not shown). In contrast, as shown in Fig. 2D, the viral proteins including ICP27, ICP5, and gB expressed throughout the slices on 5 dpi, and neuronal cell layers were clearly immunostained using anti-ICP5 antibody at this time point. Taken together, these results indicated that on 5 dpi, HSV-1 infection extensively disseminated in OHC and the neuronal cells were infected with HSV-1.

3.3. Primary disruption of neuronal cells in the hippocampus by HSV-1

To assess cellular damages caused by HSV-1 infection in the hippocampus, we immunostained the slices for NeuN (neuronal cell marker) and GFAP (astrocyte marker). As

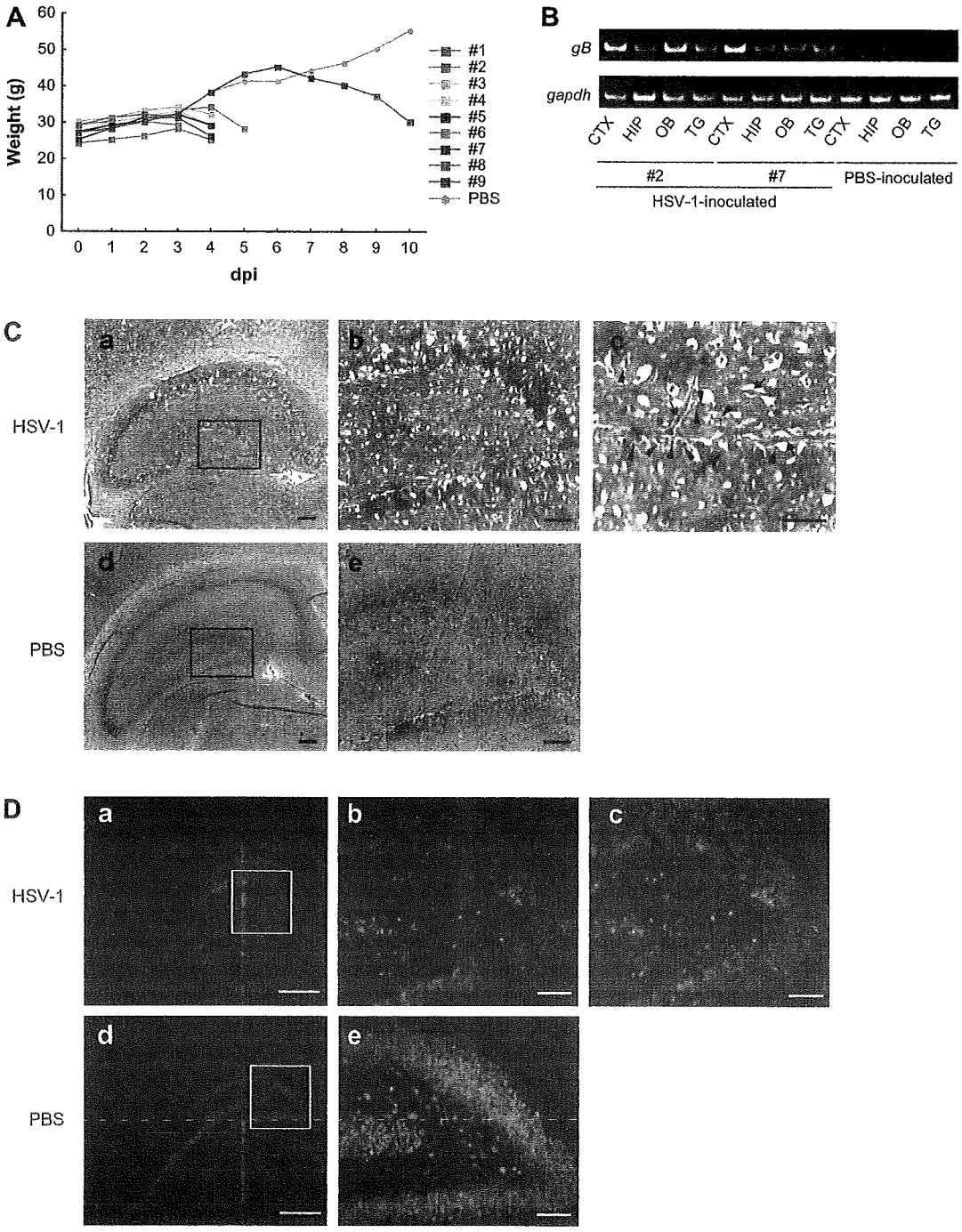

Fig. 1. Tissue damages in the hippocampus of HSV-1-infected rats. (A) Body weight of rats after HSV-1 inoculation. (B) PCR analysis using HSV-1 gB- and GAPDH-specific primers in total DNA extracted from the cerebral cortex (CTX), the hippocampus (HIP), the olfactory bulb (OB), and the trigeminal ganglia (TG). Representative results of two infected rats on 4 dpi and one PBS-inoculated rat are shown. (C) HE staining of the hippocampus in the infected rat on 10 dpi (a, b, c) or PBS-inoculated rat (d, e). Arrows indicate hemorrhagic lesions and arrowheads indicate cell infiltration. Rectangular regions in C-a and C-d are enlarged and shown in C-b and C-e, respectively. Scale bars show 300 μm (a, d), 100 μm (b, e), and 50 μm (c). (D) IHC examination for NeuN (green) and HSV-1 antigens (red) in the hippocampus of the infected rat on 10 dpi (a, b, c) or PBS-inoculated (d, e) rats. Rectangular regions in D-a and D-d are enlarged and shown in D-b, -c, and D-e, respectively. Scale bars show 500 μm (a, d) and 100 μm (b, c, e). Representative results are shown (C, D).

shown in Fig. 3, in the infected slices on 5 dpi, the numbers of NeuN antigen-expressing cells were significantly reduced, while the numbers of GFAP antigen-expressing cells were not affected. To ascertain these phenomena, we carried out IHC examination using antibodies against β-3-tubulin (B3T, neuronal cell marker), microtubule-associated protein 2 (MAP2, neuronal cell marker, expressed in cell bodies and dendrites), neurofilament protein (NFP, neuronal cell marker,

Table 1
HSV-1-induced tissue damages in the brain

Rat ID	HSV-1 inoculation	dpi	Hippocampus				Cerebral cortex				Medulla	
			Right		Left		Right		Left			
			Tissue damages[a]	Neuronal cell loss[b]	Tissue damages	Neuronal cell loss	Tissue damages	Neuronal cell loss	Tissue damages	Neuronal cell loss	Tissue damages	Neuronal cell loss
#1	+	5	+	+	+	++	+	+	+	++	+	++
#3	+	4	+	+	+	++	++	+	+	+	+	+
#5	+	4	+	+	+	++	+	+	+	+	+	+++
#9	+	10	+++	++	++	+++	++	++	++	++	++	+++
PBS	−	10	−	−	−	−	−	−	−	−	−	−

[a] The percentage of the damaged area in the coronal section is presented as follows: −, <5%; +, 5–10%; ++, 10–30%; +++, >30%.
[b] Using Image J software, NeuN intensity in the coronal section was quantified and data are shown as NeuN intensity of the brain tissue in each rat/that in PBS-inoculated rat ratio. The degree of neuronal cell loss is presented as follows: +++, <0.3; ++, 0.3–0.5; +, 0.5–0.9; −, >0.9.

expressed in axons), and S100b (astrocyte marker). Similar to Fig. 3, the numbers of B3T antigen-, MAP2 antigen-, or NFP antigen-positive neuronal cells were clearly reduced in the infected slices, while the numbers of S100b antigen-positive astrocytes in the infected slices were similar to that in uninfected slices on 5 dpi (data not shown). These results indicate that neuronal cells are more vulnerable to HSV-1-induced damages than glial cells.

Since HSV-1 is a neurotropic virus, we assumed that the vulnerability of neuronal cells to HSV-1 infection was associated with HSV-1 neurotropism. To ascertain this assumption, we carried out co-immunostaining for HSV-1 antigens and NeuN in the infected slices. We found abundant HSV-1 antigen-positive cells in CA1, CA3, and DG subfields (Fig. 4A). Identical to previous findings, NeuN antigen-positive neuronal cell layers were surrounded by GFAP antigen-positive cells [13], and NeuN expression was found in the dense clusters of nuclei [17]. It has been reported that the dense clusters of nuclei in the hippocampus correspond to neuronal cell layers [18]. In the infected slices, the dense clusters of nuclei were preserved, and were surrounded by GFAP antigen-positive cells as were in uninfected slices. However, NeuN expression was severely inhibited by HSV-1 infection (Fig. 3). In Fig. 4A, we found that large numbers of HSV-1 antigen-positive cells were located in the dense clusters of nuclei, indicating that HSV-1 infection mainly occurs in neuronal cells. Furthermore, to confirm this, we carried out co-immunostaining for ICP5 and GFAP. As shown in Fig. 4B, large numbers of ICP5 antigen-positive cells did not co-express GFAP, and they were located in the dense clusters of nuclei as similar to the results of immunostaining for HSV-1 antigens. This data indicated that HSV-1-infected and damaged cells were neuronal cells. Taken together, these results strongly suggest that HSV-1 preferentially infects neuronal cells and kills them faster than glial cells.

3.4. DG granule cells were the primary victims of HSV-1-induced tissue damages

In the hippocampus, there are 2 major classes of neuronal cells, which are pyramidal cells and granule cells. It was reported that HSV-1 antigens were frequently detected in granule cells residing in DG subfield of HSE patients [7]. To evaluate the population of neuronal cells infected with HSV-1 and to longitudinally analyze neuronal cell disruption, we used the PI uptake method and GFP-expressing HSV-1. Since this fluorescent dye rapidly intercalates into DNA of the necrotic cells losing plasma membrane integrity, we were able to detect HSV-1-induced necrosis [14]. Three days after infection with HSV-1 (YK333), we found few GFP-positive pyramidal cells in CA1 and CA3 subfields but large numbers of GFP-positive granule cells in DG subfield. At this time point, the numbers of GFP-positive cells in DG subfield were clearly larger than that in other subfields (Fig. 5A, top panels, $P < 0.05$ compared to CA1 and CA3 subfields), indicating that DG granule cells were more susceptible to HSV-1 infection than pyramidal cells. On 5 dpi, large numbers of pyramidal cells in CA1 and CA3 subfields and granule cells in DG subfield were found to be GFP positive. However, PI- and GFP-positive pyramidal cells in CA1 and CA3 subfields were a few, while numerous PI- and GFP-positive granule cells were detected in DG subfield. The numbers of PI-positive cells were also clearly higher in DG subfield (Fig. 5A, middle panels). By 10 dpi, the numbers of PI-positive cells increased in CA1, CA3, and DG subfields of the infected slices, and almost all granule cells in DG subfield became positive for PI (Fig. 5A, bottom panels). These results indicated that DG granule cells were more vulnerable to HSV-1 infection than pyramidal cells. We also examined and confirmed this with HSV-1 (F) (Fig. 5B). Taken together, these data suggest that in the hippocampus, granule cells in DG subfield are highly vulnerable to HSV-1 infection and are the primary victims of HSV-1-induced tissue damages.

4. Discussion

The mortality rate of HSE has been significantly improved because of the development of effective anti-HSV drugs. However, HSE frequently leaves its survivors with memory deficits [6]. This is due to the impairments in memory formation-associated brain tissues and it is well known that the hippocampus plays an important role for storage and recalling of information [6,15]. Although a variety of reports have been

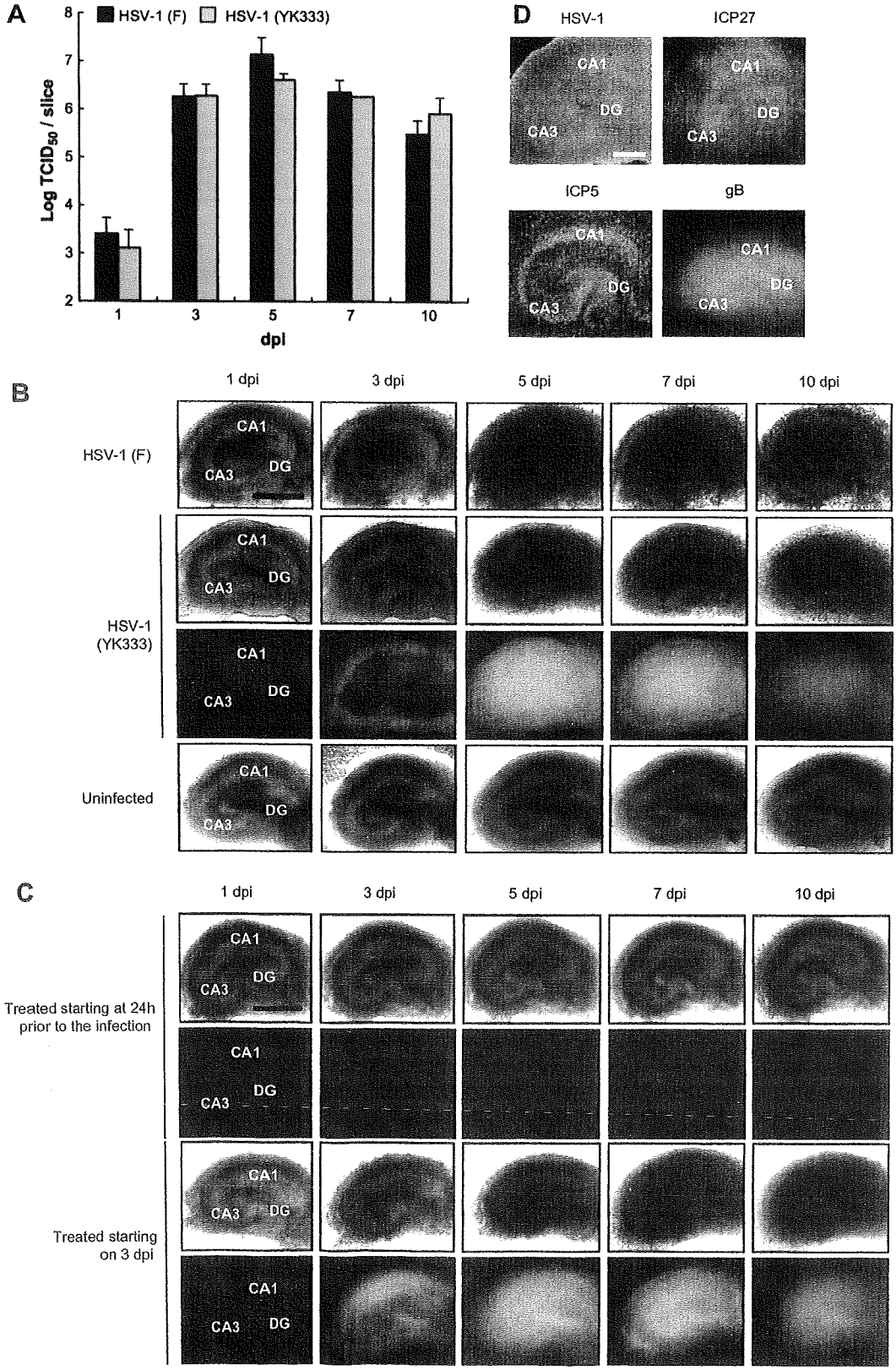

Fig. 2. Longitudinal analysis of HSV-1 infection in OHC. (A) HSV-1 titers in HSV-1 (F)-, or HSV-1 (YK333)-infected slices. Each point is represented as log $TCID_{50}$/slice ± SEM of virus titers from three independent experiments. (B) Longitudinal alterations in HSV-1-infected slices. HSV-1 (F)-infected (top panels), HSV-1 (YK333)-infected (middle panels), and uninfected (bottom panels) slices were observed up to 10 dpi. Scale bars show 1 mm. (C) Inhibition of HSV-1 replication in HSV-1 (YK333)-infected slices by acyclovir. Acyclovir treatment was started at 24 h prior to HSV-1 infection (top panels) or on third day after the infection (bottom panels). Scale bars show 1 mm. (D) IHC examination using the indicated antibodies in HSV-1 (F)-infected slices on 5 dpi. Scale bars show 500 μm. Representative results are shown (B, C, D).

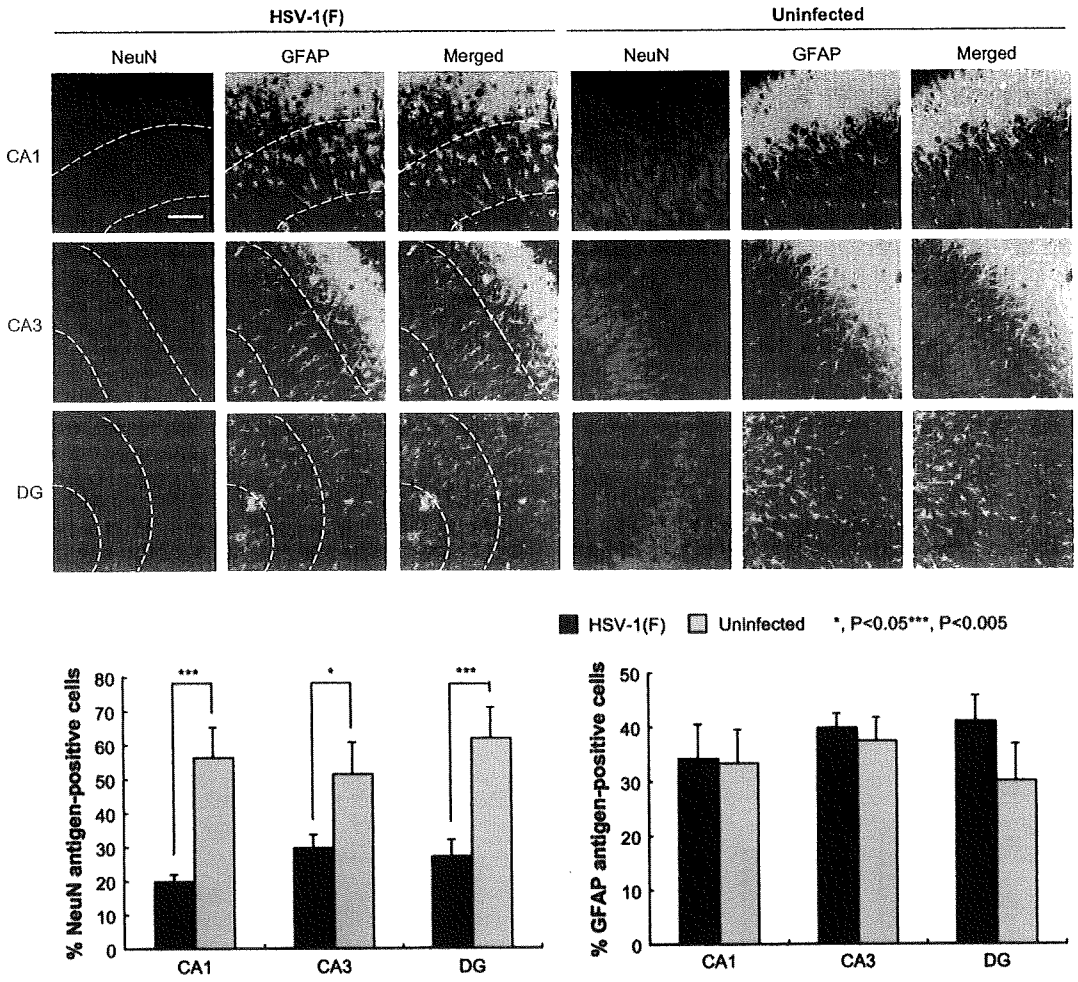

Fig. 3. Neuronal tissue damages in the hippocampus by HSV-1 infection. NeuN (red) and GFAP (green) in HSV-1 (F)-infected slices on 5 dpi or uninfected slices were co-immunostained and nuclei also were stained with Hoechst33342 (blue). The regions enclosed in the broken lines are neuronal cell layers. Scale bars show 75 μm. Representative results are shown. Quantification data were presented as the percentage of NeuN antigen-, or GFAP antigen-positive cells in Hoechst33342-stained nuclei ± SEM from three independent experiments. *, $P < 0.05$, ***, $P < 0.005$ compared to uninfected slices.

published on HSE experimental models and some have shown that HSV-1-infected mice display deficits in spatial recognition memory [19,20], the mechanism of HSV-1-induced tissue damages at the hippocampus is largely under examined. Therefore, we examined the longitudinal alteration of the hippocampus during HSV-1 infection in order to uncover the precise mechanism of hippocampal disruption.

We verified the involvement of the hippocampus in HSV-1 infection using rats intranasally inoculated with HSV-1. Our infected rats showed severe weakening with weight loss and typical clinical signs of neurological disorders (Fig. 1A). HSV-1 DNA was detected in various brain tissues, indicating that HSV-1 actually infected brain tissues of the encephalitis displaying-rats (Fig. 1B). These results are consistent with previous findings in rodent models and in humans [1,3,21]. It is known from pathological analysis of HSE autopsy samples that neuronal cells and glial cells are killed by HSV-1-induced necrosis [1,3,22]. HE-stained brain sections of our infected rats displayed focal hemorrhagic lesions and cell infiltration as well as severe cell loss in the hippocampus (Fig. 1C and Table 1). This suggests that the hippocampus of the infected rats was also mainly damaged via necrosis. In addition, Fig. 1D and Table 1 indicated that neuronal cells were severely reduced in number and that large number of HSV-1 antigen-positive cells was present in the hippocampus. These data indicate that the hippocampus is a major target tissue by HSV-1 infection.

To understand the mechanism of hippocampus disruption by HSV-1 infection, we need to carry out longitudinal evaluation of hippocampus tissue damages. However, animal models are not suitable for longitudinal analyses, especially for the investigations at the cellular level. Therefore, we used OHC. Neuronal cells and glial cells in OHC are thought to be within an microenvironment similar to that of the hippocampus in living animals [16]. Moreover, OHC has been used to elucidate some viral neuropathogenesis such as BDV and HIV-1 [9,10].

Firstly, we ascertained that HSV-1 efficiently induced tissue damages in OHC. After HSV-1 infection, the slices efficiently

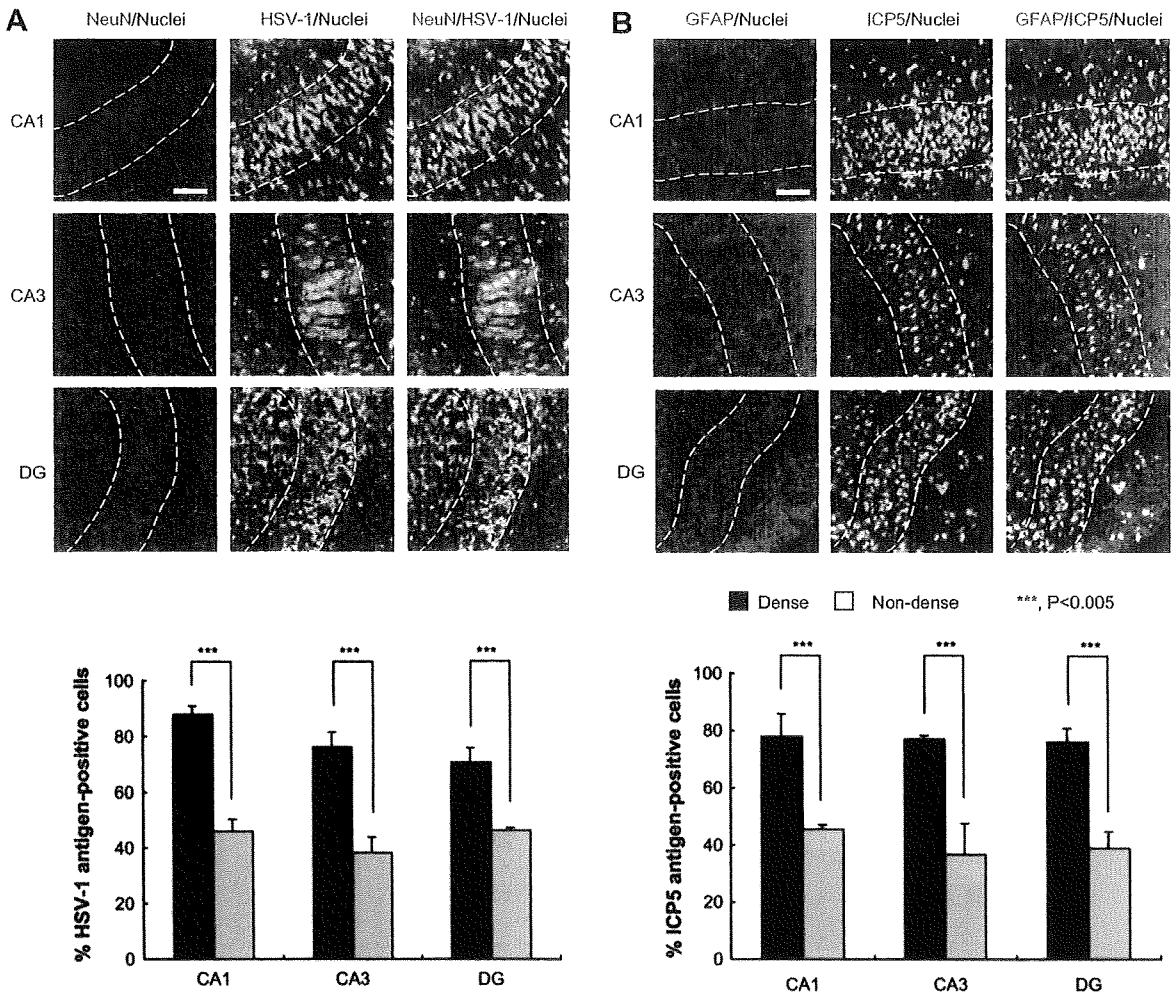

Fig. 4. HSV-1-infected cells in the hippocampus. (A) Co-immunostaining for NeuN (red) and HSV-1 antigens (green) in HSV-1 (F)-infected slices on 5 dpi. (B) Co-immunostaining for GFAP (red) and ICP5 (green) in HSV-1 (F)-infected slices on 5 dpi. Nuclei were also stained with Hoechst33342 (blue). The regions enclosed in the broken lines are the dense clusters of nuclei that indicate neuronal cell layers. Scale bars show 75 μm. Representative results are shown. Quantification data were presented as the percentage of HSV-1 antigen-, or ICP5 antigen-positive cells in Hoechst33342-stained nuclei ± SEM from three independent experiments. ***, $P < 0.005$ compared to the non-dense regions of nuclei.

released large numbers of infectious HSV-1 particles and expressed large amounts of HSV-1 proteins. As shown in Fig. 2B, HSV-1 promptly disseminated throughout the slices and the tissue architecture was gradually disrupted. Moreover, we found that HSV-1 disseminated throughout the slices on 5 dpi. These data indicate that we can evaluate HSV-1-induced hippocampal damages in vitro using OHC.

In animal models and humans, HSV-1 infection evokes immune responses such as humoral and cellular responses. After HSV-1 infection in vivo, humoral factors including complements, cytokines, and chemokines are released or activated, and macrophages, natural killer cells, dendritic cells, antigen-specific T cells, and B cells engage in the clearance of virions and virus-infected cells [23]. However, in OHC, the types of these immune cells and their numbers are limited, and consequently, virions as well as virus-infected cells would not be actively eliminated in the infected slices. As shown in Figs. 1D and 2B, there were differences in the distribution of HSV-1 antigen-positive cells between the hippocampus in vivo and the OHC. These may be explained by the differences in the presence of immune responses. OHC may have limitation of immune responses, but we think that by using OHC, we can understand the intrinsic differences in the sensitivity of hippocampal cells to HSV-1 infection.

An evaluation on cell damage by PI staining clearly demonstrated that granule cells in DG subfield were more vulnerable to HSV-1-induced damages than pyramidal cells in CA1 and CA3 subfields (Fig. 5). It has been reported that HSV-1 antigens were extensively detected in DG granule cells in autopsies of HSE patients [7], and that pronounced HSV-1 infection was observed in DG subfield of organotypic brain-slice cultures [24]. These data support our results obtained from experiments using OHC, and we concluded that DG granule cells were the primary victims of HSV-1-mediated

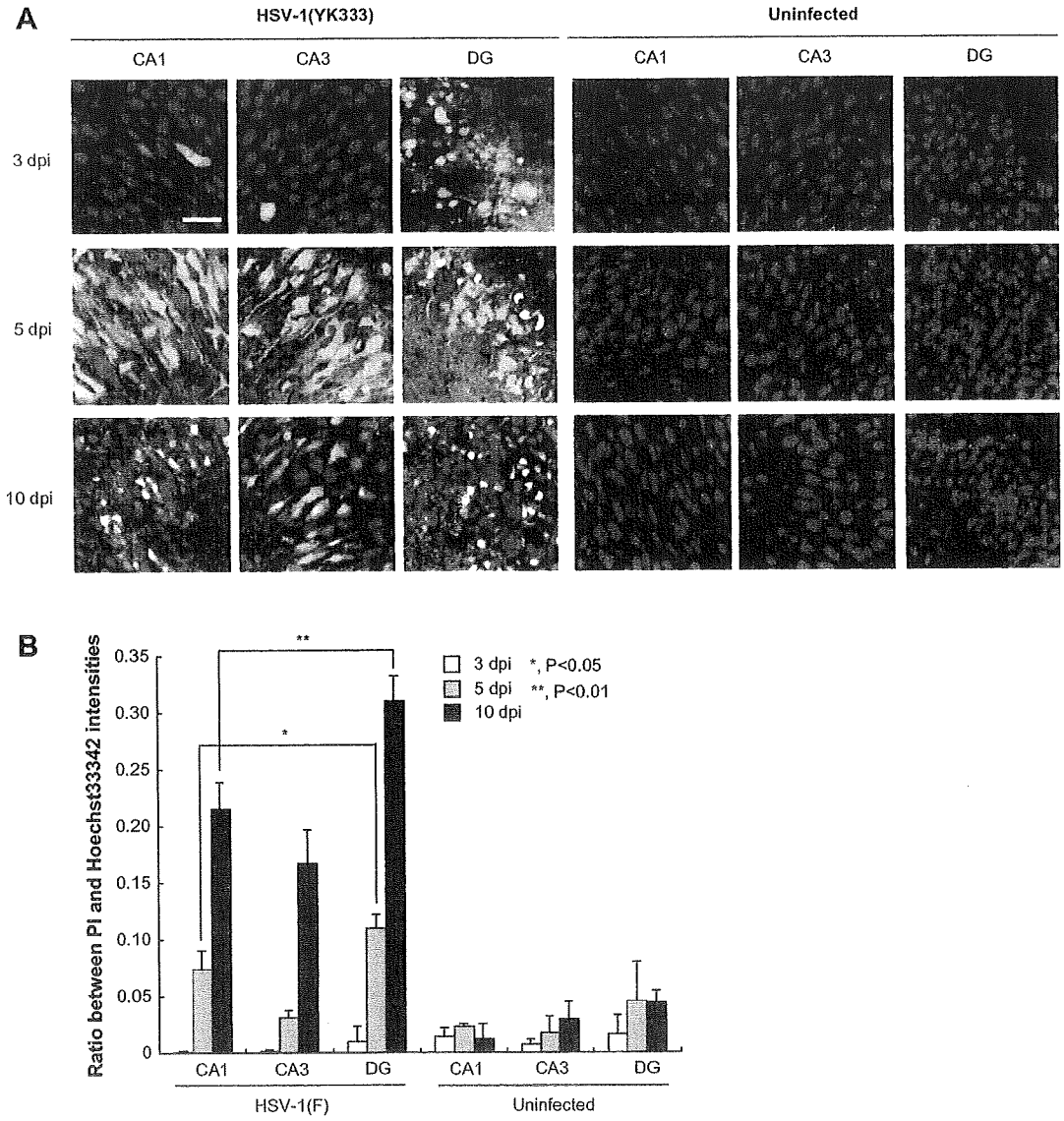

Fig. 5. Vulnerability of DG granule cells in the hippocampus. (A) Longitudinal analysis on HSV-1 (YK333)-infected slices. The infected (green) or uninfected slices were stained with PI (red) on 3, 5, and 10 dpi. Nuclei were also stained with Hoechst33342 (blue). Scale bar shows 40 μm. Representative results are shown. (B) Longitudinal analysis on HSV-1 (F)-infected slices. The infected or uninfected slices were stained with PI and Hoechst33342 on 3, 5, and 10 dpi. Using Leica software, PI intensity in each subfield was quantified. Data are presented as PI intensity/Hoechst33342 intensity ratio ± SEM from three independent experiments. *, $P < 0.05$, **, $P < 0.01$ compared to CA1 subfield of the infected slices.

cytopathic effect. Previous reports have indicated that BDV infection as well as humoral factors released from HIV-1-infected macrophages induced selective neuronal cell loss in DG granule cells [9,10,25]. Therefore, granule cells in DG subfield appear to be uniformly predisposed to virus-induced neurotoxic effects.

Acknowledgments

We thank Ms. Naoko Misawa and Mr. Chuanyi Nie for supports in our study.

This work was supported by a Grant-in-Aid for Scientific Research on Priority Areas from the Ministry of Education, Culture, Sports, Sciences, and Technology of Japan.

References

[1] R.J. Whitley, Herpes simplex encephalitis: adolescents and adults, Antiviral. Res. 71 (2006) 141–148.
[2] E. Schmutzhard, Viral infections of the CNS with special emphasis on herpes simplex infections, J. Neurol. 248 (2001) 469–477.
[3] P.G. Kennedy, A. Chaudhuri, Herpes simplex encephalitis, J. Neurol. Neurosurg. Psychiatr. 73 (2002) 237–238.
[4] P.G. Kennedy, Viral encephalitis, J. Neurol. 252 (2005) 268–272.

[5] D.H. Gilden, R. Mahalingam, R.J. Cohrs, K.L. Tyler, Herpesvirus infections of the nervous system, Nat. Clin. Pract. Neurol. 3 (2007) 82–94.
[6] L. Hokkanen, J. Launes, Cognitive outcome in acute sporadic encephalitis, Neuropsychol. Rev. 10 (2000) 151–167.
[7] M.M. Esiri, Herpes simplex encephalitis. An immunohistological study of the distribution of viral antigen within the brain, J. Neurol. Sci. 54 (1982) 209–226.
[8] R. Ellis, D. Langford, E. Masliah, HIV and antiretroviral therapy in the brain: neuronal injury and repair, Nat. Rev. Neurosci. 8 (2007) 33–44.
[9] H. Kitayama, Y. Miura, Y. Ando, Y. Koyanagi, Human immunodeficiency virus type-1 vulnerates nascent neuronal cells, Microbiol. Immunol. 52 (2008) 78–88.
[10] D. Mayer, H. Fischer, U. Schneider, B. Heimrich, M. Schwemmle, Borna disease virus replication in organotypic hippocampal slice cultures from rats results in selective damage of dentate granule cells, J. Virol. 79 (2005) 11716–11723.
[11] M. Tanaka, H. Kodaira, Y. Nishiyama, T. Sata, Y. Kawaguchi, Construction of recombinant herpes simplex virus type I expressing green fluorescent protein without loss of any viral genes, Microbes Infect 6 (2004) 485–493.
[12] S. Fujii, T. Akaike, H. Maeda, Role of nitric oxide in pathogenesis of herpes simplex virus encephalitis in rats, Virology 256 (1999) 203–212.
[13] M. Kamada, R.Y. Li, M. Hashimoto, M. Kakuda, H. Okada, Y. Koyanagi, T. Ishizuka, H. Yawo, Intrinsic and spontaneous neurogenesis in the postnatal slice culture of rat hippocampus, Eur. J. Neurosci. 20 (2004) 2499–2508.
[14] O. Chechneva, K. Dinkel, F. Cavaliere, M. Martinez-Sanchez, K.G. Reymann, Anti-inflammatory treatment in oxygen-glucose-deprived hippocampal slice cultures is neuroprotective and associated with reduced cell proliferation and intact neurogenesis, Neurobiol. Dis. 23 (2006) 247–259.
[15] G. Neves, S.F. Cooke, T.V. Bliss, Synaptic plasticity, memory and the hippocampus: a neural network approach to causality, Nat. Rev. Neurosci. 9 (2008) 65–75.
[16] B.H. Gahwiler, M. Capogna, D. Debanne, R.A. McKinney, S.M. Thompson, Organotypic slice cultures: a technique has come of age, Trends Neurosci. 20 (1997) 471–477.
[17] R.J. Mullen, C.R. Buck, A.M. Smith, NeuN, a neuronal specific nuclear protein in vertebrates, Development 116 (1992) 201–211.
[18] E. Forster, S. Zhao, M. Frotscher, Laminating the hippocampus, Nat. Rev. Neurosci. 7 (2006) 259–267.
[19] J.H. McLean, M.T. Shipley, D.I. Bernstein, D. Corbett, Selective lesions of neural pathways following viral inoculation of the olfactory bulb, Exp. Neurol. 122 (1993) 209–222.
[20] D.R. Beers, J.S. Henkel, R.P. Kesner, W.G. Stroop, Spatial recognition memory deficits without notable CNS pathology in rats following herpes simplex encephalitis, J. Neurol. Sci. 131 (1995) 119–127.
[21] Y. Becker, HSV-1 brain infection by the olfactory nerve route and virus latency and reactivation may cause learning and behavioral deficiencies and violence in children and adults: a point of view, Virus Genes 10 (1995) 217–226.
[22] L.E. Davis, R.T. Johnson, An explanation for the localization of herpes simplex encephalitis? Ann. Neurol. 5 (1979) 2–5.
[23] H. Wakimoto, P.R. Johnson, D.M. Knipe, E.A. Chiocca, Effects of innate immunity on herpes simplex virus and its ability to kill tumor cells, Gene Ther. 10 (2003) 983–990.
[24] E. Braun, T. Zimmerman, T.B. Hur, E. Reinhartz, Y. Fellig, A. Panet, I. Steiner, Neurotropism of herpes simplex virus type 1 in brain organ cultures, J. Gen. Virol. 87 (2006) 2827–2837.
[25] K.M. Carbone, S.W. Park, S.A. Rubin, R.W. Waltrip 2nd, G.B. Vogelsang, Borna disease: association with a maturation defect in the cellular immune response, J. Virol. 65 (1991) 6154–6164.

JOURNAL OF VIROLOGY, Dec. 2008, p. 11958–11963 Vol. 82, No. 23
0022-538X/08/$08.00+0 doi:10.1128/JVI.01149-08

NOTES

Critical Role for TSLC1 Expression in the Growth and Organ Infiltration of Adult T-Cell Leukemia Cells In Vivo▽

M. Zahidunnabi Dewan,[1,2]† Naofumi Takamatsu,[3] Tomonori Hidaka,[4] Kinta Hatakeyama,[5] Shingo Nakahata,[3] Jun-ichi Fujisawa,[6] Harutaka Katano,[7] Naoki Yamamoto,[1,2]* and Kazuhiro Morishita[3]*

Department of Molecular Virology, Graduate School, Tokyo Medical and Dental University, 1-5-45 Yushima, Bunkyo-ku, Tokyo 113-8519, Japan[1]; AIDS Research Center, National Institute of Infectious Disease, 1-23-1 Toyama, Shinjuku-ku, Tokyo 162-8640, Japan[2]; Department of Medical Sciences,[3] Department of Internal Medicine,[4] and Department of Pathology,[5] Faculty of Medicine, University of Miyazaki, Kiyotake, Miyazaki, Japan; Department of Microbiology, Kansai Medical University, Moriguchi, Osaka, Japan[6]; and Department of Pathology, National Institute of Infectious Diseases, 1-23-1 Toyama, Shinjuku-ku, Tokyo 162-8640, Japan[7]

Received 2 June 2008/Accepted 15 September 2008

Adult T-cell leukemia (ATL) is associated with human T-cell leukemia virus type 1 infection. The tumor suppressor lung cancer 1 (TSLC1) gene was previously identified as a novel cell surface marker for ATL, and this study demonstrated the involvement of TSLC1 expression in tumor growth and organ infiltration of ATL cells. In experiments using NOD/SCID/γc^{null} mice, both leukemia cell lines and primary ATL cells with high TSLC1 expression caused more tumor formation and aggressive infiltration of various organs of mice. Our results suggest that TSLC1 expression in ATL cells plays an important role in the growth and organ infiltration of ATL cells.

Human T-cell leukemia virus type 1 (HTLV-1) is the causative agent of an aggressive form of $CD4^+$ T-cell leukemia termed adult T-cell leukemia (ATL) (7, 14, 18). Carriers of HTLV-1 have been identified in a number of locations throughout the world, including parts of Africa; Papua New Guinea; specific regions in Europe including Romania; parts of South America including northern Brazil, Peru, northern Argentina, and Colombia; and the southern part of Kyushu in Japan (17). Common findings in patients with ATL include enlargement of peripheral lymph nodes, hepatomegaly, splenomegaly, skin infiltration, and hypercalcemia. The Tax gene is a unique viral gene thought to play a central role in HTLV-1-induced transformation. It is responsible for transactivation of the HTLV-1 long terminal repeat (5, 16) and numerous cellular genes involved in T-cell activation and growth, including those encoding interleukin-2 (IL-2) (11) and the α chain of IL-2 receptor (IL-2Rα) (CD25, Tac) (1, 2). The long latency of ATL development suggests that multiple genetic events accumulate in HTLV-1-infected cells; however, the precise molecular mechanisms of ATL leukemogenesis following HTLV-1 infection have not been fully elucidated.

The tumor suppressor lung cancer 1 gene (TSLC1) at chromosome 11q23 has been identified as a tumor suppressor gene in non-small-cell lung cancer (9, 13). In contrast, it was recently found to be highly and ectopically expressed in acute-type ATL cells, most ATL cell lines, and HTLV-1-infected T-cell lines (15). Enforced expression of TSLC1 in ATL-derived ED-40515(−) cells resulted in higher aggregations and binding abilities in a human umbilical vein endothelial cell line (HUVEC). These results suggest that TSLC1 might contribute to tumor growth by enhancing aggregation after infiltration and migration outside blood vessels. Since the role of TSLC1 overexpression in the course of tumor growth and organ infiltration of ATL cells remains to be fully elucidated, we investigated the direct involvement of TSLC1 in the growth and infiltration of leukemia cells using C57BL/6J and NOD-SCID/γc^{null} (NOG) mice (4, 8).

In order to analyze the tumorigenicity of TSLC1 expression in leukemia cells, a murine IL-2-independent T-lymphoma cell line (EL4) injected into the intraperitoneum of syngeneic C57BL/6J mice was used as a model for ATL. EL4 cells were transfected with a pcDNA3 expression plasmid containing TSLC1, and transformant cells were selected by a limiting-dilution method in the presence of G-418. We also used EL4 cells expressing a green fluorescent protein-Tax fusion protein (EL4/GAX) (6) and parental EL4 (EL4/p) as a control. Expression of Tax protein in EL4 cells, a 38-kDa band of Tax protein in HUT102 cells, and a 64-kDa band of green fluorescent protein-Tax fusion protein in EL4/GAX cells were all

* Corresponding author. Mailing address for Naoki Yamamoto: AIDS Research Center, National Institute of Infectious Disease, 1-23-1 Toyama, Shinjuku-ku, Tokyo 162-8640, Japan. Phone: 81-3-5285-1111. Fax: 81-3-5285-1165. E-mail: nyama@nih.go.jp. Mailing address for Kazuhiro Morishita: Division of Tumor and Cellular Biochemistry, Department of Medical Sciences, Faculty of Medicine, University of Miyazaki, Kiyotake, Miyazaki, Japan. Phone: 81-9-8585-0985. Fax: 81-9-8585-2401. E-mail: kmorishi@med.miyazaki-u.ac.jp.

† Present address: Department of Pathology, New York University School of Medicine, 550 First Avenue, New York, NY 10016.

▽ Published ahead of print on 15 October 2008.

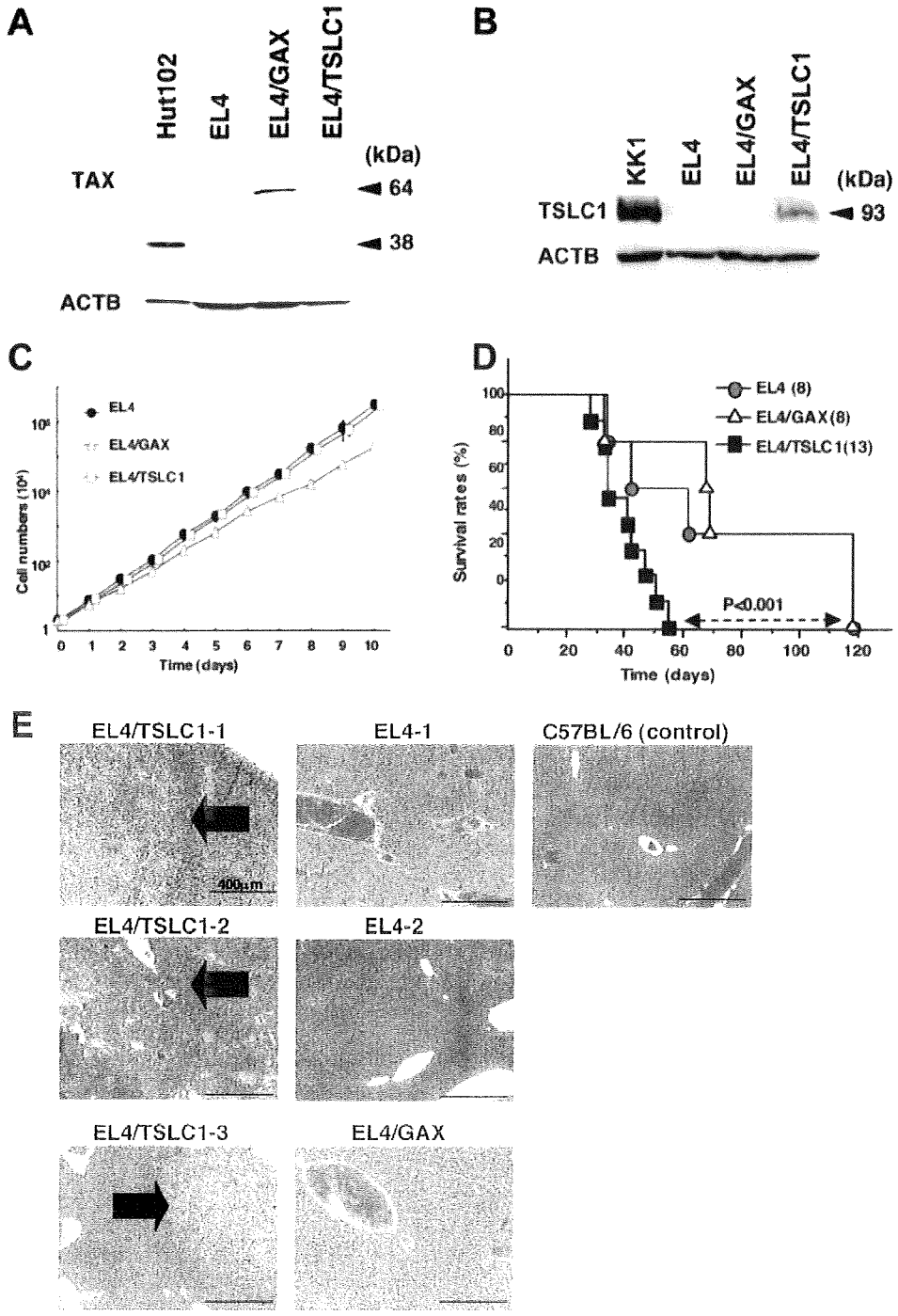

FIG. 1. Transplantation of EL4 T-cell lymphoma cells expressing TSLC1 shortened the life span of syngeneic mice. (A) Expression of Tax protein in HUT102, EL4, EL4/GAX, and EL4/TSLC1 cells was detected by Western blot analysis. Expression of β-actin protein (ACTB) was used as a loading control. (B) Expression of TSLC1 protein in KK1, EL4, EL4/GAX, and EL4/TSLC1 cells was detected by Western blot analysis. Expression of β-actin protein (ACTB) was used as a loading control. (C) Cell numbers in a growth curve are shown for an average of three independent counts, and standard deviations are indicated as error bars. (D) Survival curves of C57BL/6 mice inoculated in the abdominal cavity with EL4, EL4/GAX, or EL4/TSLC1 cells. Cumulative survival rates were calculated by the Kaplan-Meier method and compared using a log-rank test. (E) Liver sections from all mice were stained with hematoxylin-eosin. The regions of liver metastasis (arrow) were seen in liver sections from mice inoculated with EL4/TSLC1 cells but not shown in the liver sections from the mice inoculated with EL4 or EL4/GAX cells. Magnification, ×100; bars, 400 μm.

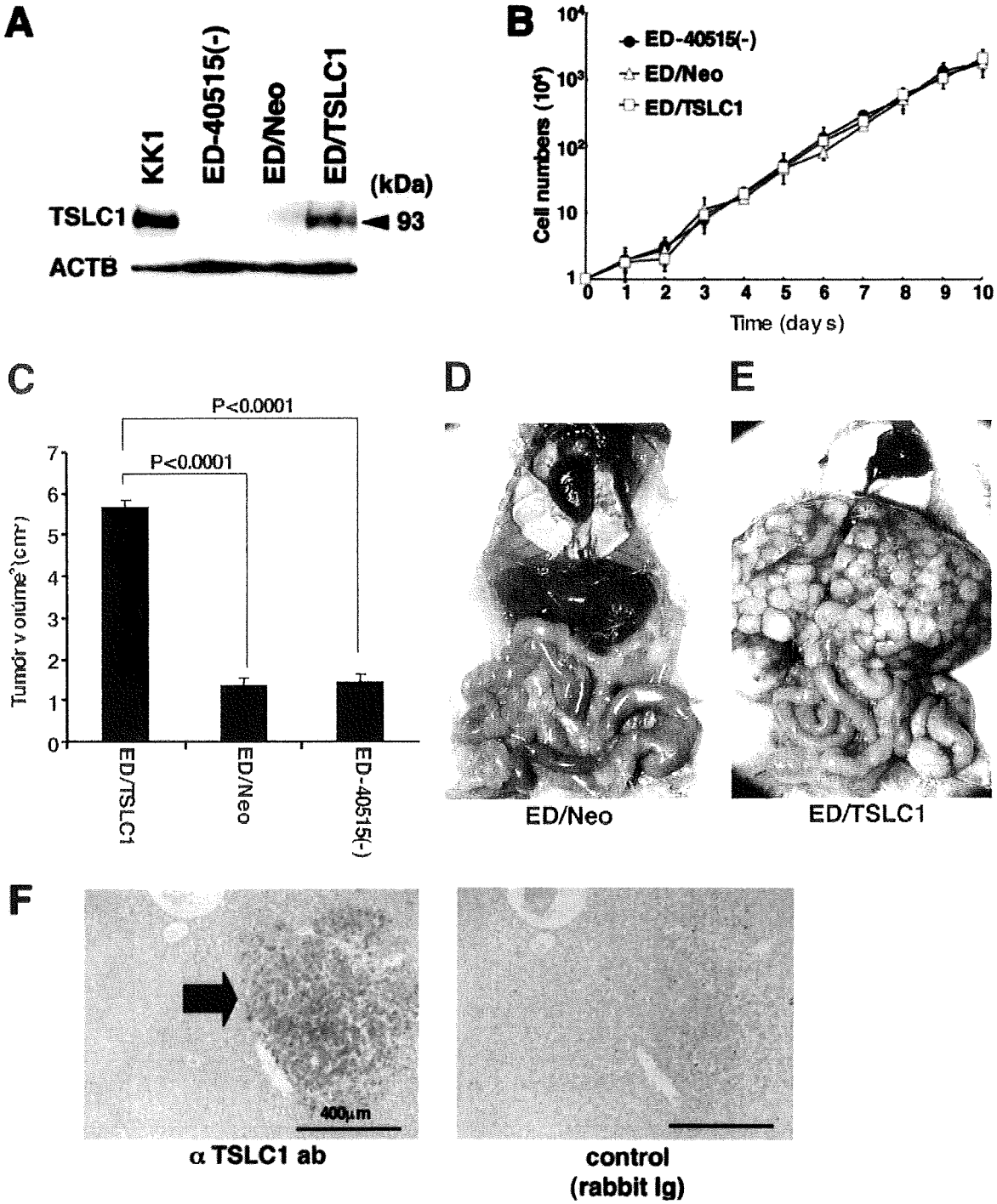

FIG. 2. Involvement of TSLC1 expression in tumor growth and infiltration of leukemia cells in NOG mice. (A) Expression of TSLC1 in KK1, ED-40515(−), ED/Neo, or ED/TSLC1 cell lines was detected by Western blot analysis. Expression of β-actin protein (ACTB) was used as a loading control. (B) Cell growth curves of ED-40515(−), ED/Neo, and ED/TSLC1 cell lines are shown for an average of three independent counts, and standard deviations are indicated as error bars. (C) Tumor volumes of mice inoculated subcutaneously with ED/TSLC1, ED/Neo, or ED-40515(−) cells after 21 days are shown as the means ± standard errors of the means for five mice in each group. Statistical analysis was done with a Student *t* test. (D and E) The pictures shown were derived from gross photographs of the sacrificed mice at 1 month after intravenous inoculation of ED/Neo (D) or ED/TSLC1 (E) cells. (F) Immunohistochemical staining for TSLC1 protein in liver metastases of the mice inoculated intravenously with ED/TSLC1 cells is shown. An arrow indicates a tumor mass with strong staining with a rabbit anti-TSLC1 antibody; however, the same mass shows no staining with rabbit immunoglobulin (Ig) as a negative control. Magnification, ×100; bars, 400 μm.

TABLE 1. Invasion scores of mice inoculated with ED/Neo or ED/TSLC1 cells

Cell line and mouse	Invasion score for organ by observation:									
	Macroscopic[a]					Microscopic[b]				
	Liver	Kidney	Lung	Ovary	Spleen	Liver	Kidney	Lung	Ovary	Spleen
ED/TSLC1										
T1	3+	−	+/−	1+	−	3+	−	2+	2+	−
T2	3+	−	−	1+	−	3+	−	2+	2+	−
T3	3+	−	+/−	2+	−	3+	−	2+	2+	−
T4	3+	−	−	1+	−	3+	−	2+	2+	−
T5	2+	−	−	2+	−	3+	−	2+	3+	−
T6	3+	−	+/−	1+	−	3+	−	+/−	2+	−
ED/Neo										
N1	−	−	−	2+	−	2+	−	+/−	3+	−
N2	+/−	−	−	1+	−	+/−	−	−	2+	−
N3	−	−	−	2+	−	−	−	+/−	2+	−
N4	−	−	−	1+	−	−	−	−	2+	−
N5	−	−	−	1+	−	ND[c]	ND	ND	ND	ND
N6	−	−	−	1+	−	ND	ND	ND	ND	ND

[a] Subjective invasion scores by macroscopic observation were as follows: −, no invasion; +/−, less than 10% invasion in the organ; 1+, 10 to 30% invasion in the organ; 2+, 30 to 70% invasion in the organ; 3+, over 70% invasion in the organ.

[b] Subjective invasion scores by microscopic observation were as follows: −, no invasion; +/−, less than 1% leukemia cells in the section; 1+, less than 10% leukemia cells in the section; 2+, 10 to 30% leukemia cells in the section; 3+, over 30% leukemia cells in the section

[c] ND, not done.

detected by Western blot analysis (Fig. 1A). Expression of a TSLC1 protein in EL4/TSLC1 cells was also shown on Western blot analysis with KK1, an ATL cell line expressing TSLC1 (12) (Fig. 1B). In an in vitro cell growth assay, 2×10^4 cells were incubated, and their growth was analyzed by direct counting with trypan blue dye staining. EL4 and EL4/TSLC1 cells showed nearly identical proliferation profiles in vitro, while Tax-expressing EL4 cells proliferated more slowly (Fig. 1C). This difference in cell growth might be caused by different expression vectors. In an in vivo growth assay, 2×10^6 cells of each cell line were injected into the peritoneal cavity of C57BL/6J mice: eight mice for EL4 cells as controls, 13 mice for EL4/TSLC1 cells, and eight mice for EL4/GAX cells. All of the mice died of tumor invasion of various organs with ascitic fluids in 40 to 120 days. The median survival time of the control mice injected with EL4 cells or EL4/GAX cells was 72 days. The mice with EL4/TSLC1 cells, however, died within 60 days, with a median survival time of 41 days (Fig. 1D). The phenotypes of the control mice and the EL4/TSLC1 mice were almost identical with invasion of tumors into various organs. Organ metastasis of tumor cells in three EL4/TSLC1-inoculated mice, two EL4-inoculated mice, and one EL4/GAX-inoculated mouse was analyzed and evaluated with hematoxylin-eosin staining. The liver was one of the major sites of metastasis in all three of the EL4/TSLC1-inoculated mice by histopathological analysis but not in the two EL4-inoculated mice or the EL4/GAX-inoculated mouse (Fig. 1E). These results support the role of TSLC1 overexpression in T-lymphoma cells as one of an aggressive factor in the development of leukemia/lymphoma.

In order to investigate the possibility that overexpression of TSLC1 promotes tumor growth and/or infiltration in vivo,

TABLE 2. Clinical characteristics of patients and pathological findings of organ invasion[a]

Patient no.	Age (yr)/sex	Clinical characteristic				Invasion score in NOG mice[b]				TSLC1 expression score[c]
		Diagnosis (ATL type)	WBC (10^9/liter)	Lymphocytes (%)	Atypical cells (%)	Liver	Lung	Spleen	Lymph node	
1	73/M	Chronic	7.8	59	47	3+	3+	3+	ND	3+
2	59/F	Chronic	9.0	75	40	3+	2+	2+	1+	2+
3	66/F	Chronic	29.4	49	75	3+	3+	3+	ND	3+
4	44/F	Chronic	22.6	51	45	3+	2+	2+	2+	2+
5	43/F	Chronic	18.6	63	43	3+	3+	3+	ND	2+
6	54/M	Acute	192.8	65	91	1+	2+	ND	ND	1+
7	58/M	Acute	67.3	71	80	3+	3+	3+	ND	2+
8	65/F	Acute	29.4	25	60	3+	2+	ND	3+	3+
9	68/M	Acute	30.0	79	81	3+	1+	1+	2+	2+
10	66/F	Acute	10.2	38	51	3+	3+	3+	ND	3+

[a] Abbreviations: M, male; F, female; WBC, white blood cells; ND, not done.

[b] Subjective invasion scores were as follows: 0, no invasion; 1+, less than 10% leukemia cells in the section; 2+, 10 to 30% leukemia cells in the section; 3+, over 30% leukemia cells in the section.

[c] Subjective scores of TSLC1 expression in pathological immunostaining were as follows; −, no staining; 1+, faint staining in less than 10% of invasive leukemia cells; 2+, weak to moderate staining in 30 to 70% of invasive leukemia cells; 3+, intense staining in more than 70% of invasive leukemia cells.

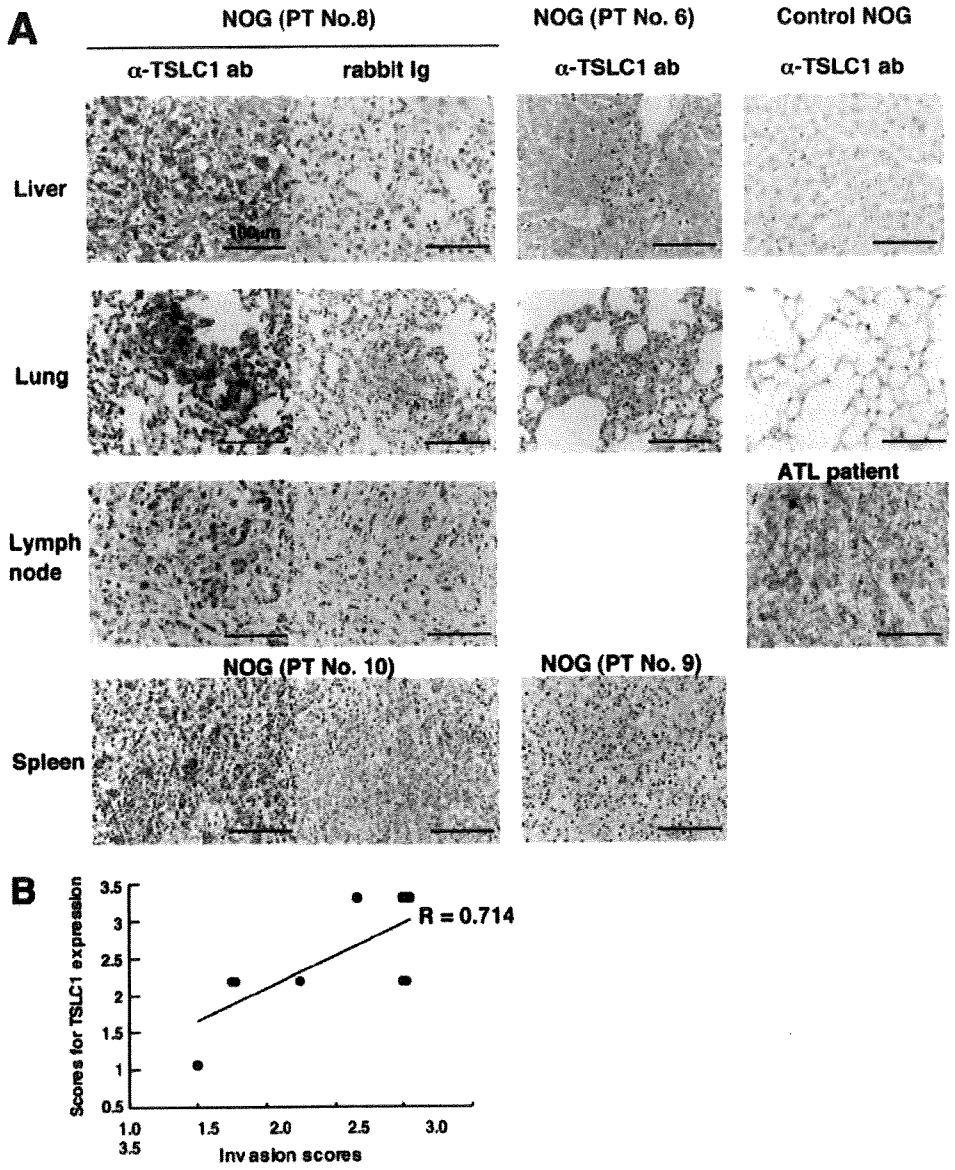

FIG. 3. Growth and infiltration of primary ATL cells in various organs of NOG mice based on TSLC1 expression. (A) Immunohistochemical staining of various organs of NOG mice inoculated with leukemia cells from patient 6, 8, 9, or 10 is shown with the use of rabbit anti-TSLC1 antibody or rabbit immunoglobulin (Ig) as a negative control. Sections from patients 8 and 10 showed severe invasion (invasion score, 3) and dense staining for TSLC1 (expression score, 3), while sections from patients 6 and 9 showed mild invasion (invasion score, 1) and light staining for TSLC1 (expression score, 1). Liver and lung sections from control NOG mice were used as negative controls, and a lymph node from an ATL patient was used as a positive control. Magnification, ×400; bars, 100 μm. (B) The diagram of dispersion between mean values of each invasion score and scores for TSLC1 expression in each NOG mouse inoculated with primary ATL cells showed moderate correlation (R = 0.714).

ATL-derived ED-40515(−) cells (10) were injected into NOG mice. Since expression of TSLC1 in ED-40515(−) cells is severely reduced by promoter methylation, they were transfected with either a TSLC1 expression plasmid (pcDNA3/TSLC1) or a mock plasmid (pcDNA3/Neo). ED/TSLC1 and ED/Neo cells were identified by selection with G-418. High levels of TSLC1 expression were verified in the ED/TSLC1 cells, but not in the ED/Neo cells, by Western blot analysis (Fig. 2A). The ED/TSLC1, ED/Neo, and ED-40515(−) cell lines all showed the same proliferation profile in vitro (Fig. 2B). Cells (10×10^6) were inoculated subcutaneously into the postauricular region of NOG mice, which permitted the observation of tumor growth macroscopically and the measurement of tumor size over a relatively short time (3). The ED/TSLC1 cell lines caused greater formation of larger tumors than did the ED/Neo and ED-40515(−) cell lines (Fig. 2C). The development of clinical signs of near-death (e.g., piloerection, weight loss, and cachexia) in mice at the time of killing was also more prevalent with the ED/TSLC1 cell line. These results suggest that TSLC1 expression in ATL cells enhances in vivo tumor growth in NOG mice.

Since the mice died within 4 weeks after subcutaneous in-

oculation of leukemia cells due to heavy tumor burden, 2×10^6 ED/TSLC1 or ED/Neo cells were intravenously injected into six NOG mice in order to investigate their capacity for invasion of various organs. After 1 month, we sacrificed the mice to determine the extent of organ invasion. Macroscopically, all of the mice injected with ED/TSLC1 cells (six/six) showed severe liver invasion with swelling of the ovaries. None of the mice injected with ED/Neo cells showed liver invasion, but they did show ovarian involvement (Fig. 2D and E). Microscopically, all of the mice inoculated with ED/TSLC1 cells showed severe and massive liver and lung invasions. On the other hand, only one of six mice inoculated with ED/Neo cells showed a large amount of liver metastasis (Table 1). TSLC1 expression in tumor cells infiltrating the liver was confirmed by immunohistochemical staining (Fig. 2F). Thus, overexpression of TSLC1 in ATL cells might enhance organ invasion, and particularly invasion of the liver and lung.

Next, we examined whether primary ATL cells with various levels of expression of TSLC1 could efficiently grow and infiltrate various organs in NOG mice. TSLC1-positive primary ATL cells (2×10^7) from five acute-type and five chronic-type ATL patients were inoculated subcutaneously into the postauricular region of NOG mice (Table 2). All of the mice developed clinical signs of near-death (e.g., piloerection, weight loss, and cachexia) 6 to 8 weeks after inoculation, in addition to the enlargement of the lymph nodes, spleen, lungs, and liver. Microscopically, ATL cells invaded various organs of all ATL-bearing NOG mice to different degrees. Based on results of immunohistochemical staining for TSLC1, all invading leukemia cells expressed TSLC1 protein, compared with no TSLC1 expression in these organs in control NOG mice (Table 2 and Fig. 3A). The dispersion diagram for the levels of invasion and the levels of TSLC1 expression in the leukemia cells showed a correlation coefficient of 0.714, suggesting that there was a moderate correlation between invasive capability and the level of TSLC1 expression (Fig. 3B). Thus, TSLC1 could aid in the formation of a rapidly growing large tumor and massive infiltration of ATL cells into various organs in NOG mice. Since TSLC1 is expressed in various types of ATL cells, including smoldering and chronic types, it might be a promising target for the development of a new anti-ATL therapy. The NOG mouse model system described in the present study could provide a novel means by which to understand and investigate the further importance of TSLC1 in ATL progression.

We thank S. Ichinose of the Instrumental Analysis Research Center; S. Endo of the Animal Research Center, Tokyo Medical and Dental University; and Y. Sato of the National Institute of Infectious Diseases for her excellent technical assistance. Anti-Tax (MI73) antibody was the kind gift of Y. Namba and M. Matsuoka (Institute for Virus Research, Kyoto University).

Supported by grants from the Ministry of Education, Science, and Culture; the Ministry of Health, Labor, and Welfare; and Human Health Science of Japan.

REFERENCES

1. **Ballard, D. W., E. Bohnlein, J. W. Lowenthal, Y. Wano, B. R. Franza, and W. C. Greene.** 1988. HTLV-I tax induces cellular proteins that activate the B element in the IL-2 receptor gene. Science **241**:1652–1655.
2. **Cross, S. L., M. B. Feinberg, J. B. Wolf, N. J. Holbrook, F. Wong-Staal, and W. J. Leonard.** 1987. Regulation of the human interleukin-2 receptor chain promoter: activation of a nonfunctional promoter by the transactivator gene of HTLV-I. Cell **49**:47–56.
3. **Dewan, M. Z., K. Terashima, M. Taruishi, H. Hasegawa, M. Ito, Y. Tanaka, N. Mori, T. Sata, Y. Koyanagi, M. Maeda, Y. Kubuki, A. Okayama, M. Fujii, and N. Yamamoto.** 2003. Rapid tumor formation of human T-cell leukemia virus type 1-infected cell lines in novel NOD-SCID/$c\gamma^{null}$ mice: suppression by an inhibitor against NF-κB. J. Virol. **77**:5286–5294.
4. **Dewan, M. Z., J. N. Uchihara, K. Terashima, M. Honda, T. Sata, M. Ito, N. Fujii, K. Uozumi, K. Tsukasaki, M. Tomonaga, Y. Kubuki, A. Okayama, M. Toi, N. Mori, and N. Yamamoto.** 2006. Efficient intervention of growth and infiltration of primary adult T-cell leukemia cells by an HIV protease inhibitor, ritonavir. Blood **107**:716–724.
5. **Felber, B. K., H. Paskalis, C. Kleinman-Ewing, F. Wong-Staal, and G. N. Pavlakis.** 1985. The pX protein of HTLV-I is a transcriptional activator of its long terminal repeats. Science **229**:675–679.
6. **Furuta, R. A., K. Sugiura, S. Kawakita, T. Inada, S. Ikehara, T. Matsuda, and J. Fujisawa.** 2002. Mouse model for the equilibration interaction between the host immune system and human T-cell leukemia virus type 1 gene expression. J. Virol. **76**:2703–2713.
7. **Hinuma, Y., K. Nagata, M. Hanaoka, M. Nakai, T. Matsumoto, K. I. Kinoshita, S. Shirakawa, and I. Miyoshi.** 1981. Adult T-cell leukemia: antigen in an ATL cell line and detection of antibodies to the antigen in human sera. Proc. Natl. Acad. Sci. USA **78**:6476–6480.
8. **Ito, M., H. Hiramatsu, K. Kobayashi, K. Suzue, M. Kawahata, K. Hioki, Y. Ueyama, Y. Koyanagi, K. Sugamura, K. Tsuji, T. Heike, and T. Nakahata.** 2002. NOD/SCID/.cnull mouse: an excellent recipient mouse model for engraftment of human cells. Blood **100**:3175–3182.
9. **Kuramochi, M., H. Fukuhara, T. Nobukuni, T. Kanbe, T. Maruyama, H. P. Ghosh, M. Pletcher, M. Isomura, M. Onizuka, T. Kitamura, T. Sekiya, R. H. Reeves, and Y. Murakami.** 2001. TSLC1 is a tumor suppressor gene in human non-small cell lung cancer. Nat. Genet. **27**:427–730.
10. **Maeda, M., A. Shimizu, K. Ikuta, H. Okamoto, M. Kashihara, T. Uchiyama, T. Honjo, and J. Yodoi.** 1985. Origin of human T-lymphotrophic virus I-positive T cell lines in adult T cell leukemia. Analysis of T cell receptor gene rearrangement. J. Exp. Med. **162**:2169–2174.
11. **Maruyama, M., H. Shibuya, H. Harada, M. Hatakeyama, M. Seiki, T. Fujita, J. Inoue, M. Yoshida, and T. Taniguchi.** 1987. Evidence for aberrant activation of the interleukin-2 autocrine loop by HTLV-1-encoded p40x and T3/Ti complex triggering. Cell **48**:343–350.
12. **Masuda, M., M. Yagita, H. Fukuhara, M. Kuramochi, T. Maruyama, A. Nomoto, and Y. Murakami.** 2002. The tumor suppressor protein TSLC1 is involved in cell-cell adhesion J. Biol. Chem. **277**:31014–31019.
13. **Murakami, Y., T. Nobukuni, K. Tamura, T. Maruyama, T. Sekiya, Y. Arai, H. Gomyou, A. Tanigami, M. Ohki, D. Cabin, P. Frischmeyer, P. Hunt, and R. H. Reeves.** 1998. Localization of tumor suppressor activity important in non-small cell lung carcinoma on chromosome 11q. Proc. Natl. Acad. Sci. USA **95**:8153–8158.
14. **Poiesz, B. J., F. W. Ruscetti, A. F. Gazdar, P. A. Bunn, J. D. Minna, and R. C. Gallo.** 1980. Detection and isolation of type C retrovirus particles from fresh and cultured lymphocytes of a patient with cutaneous T-cell lymphoma. Proc. Natl. Acad. Sci. USA **77**:7415–7419.
15. **Sasaki, H., I. Nishikata, T. Shiraga, E. Akamatsu, T. Fukami, T. Hidaka, Y. Kubuki, A. Okayama, K. Hamada, H. Okabe, Y. Murakami, H. Tsubouchi, and K. Morishita.** 2005. Overexpression of a cell adhesion molecule, TSLC1, as a possible molecular marker for acute type of adult T-cell leukemia. Blood **105**:1204–1213.
16. **Sodroski, J. G., C. A. Rosen, and W. A. Haseltine.** 1984. Transacting transcriptional activation of the long terminal repeat of human T lymphotropic viruses in infected cells. Science **225**:381–385.
17. **Yamaguchi, K., and T. Watanabe.** 2002. Human T lymphotropic virus type-I and adult T-cell leukemia in Japan. Int. J. Hematol. **76**:240–245.
18. **Yoshida, M., I. Miyoshi, and Y. Hinuma.** 1982. Isolation and characterization of retrovirus from cell lines of human adult T-cell leukemia and its implication in the disease. Proc. Natl. Acad. Sci. USA **79**:2031–2035.

ELSEVIER

INSTITUT PASTEUR

Microbes and Infection 10 (2008) 748–756

www.elsevier.com/locate/micinf

Original article

Induction of apoptosis in Epstein-Barr virus-infected B-lymphocytes by the NF-κB inhibitor DHMEQ

Ariko Miyake [a,1], Md. Zahidunnabi Dewan [b,c,1], Takaomi Ishida [a], Mariko Watanabe [d], Mitsuo Honda [c], Tetsutaro Sata [e], Naoki Yamamoto [b,c,**], Kazuo Umezawa [f], Toshiki Watanabe [a,***], Ryouichi Horie [d,*]

[a] *Laboratory of Tumor Cell Biology, Department of Medical Genome Sciences, Graduate School of Frontier Sciences, University of Tokyo, 4-6-1 Shirokanedai, Minato-ku, Tokyo 108-8639, Japan*

[b] *Department of Molecular Virology, Bio-Response, Graduate School, Tokyo Medical and Dental University, 1-5-45 Yushima, Bunkyo-ku, Tokyo 113-8519, Japan*

[c] *AIDS Research Center, National Institute of Infectious Diseases, 1-23-1 Toyama, Shinjuku-ku, Tokyo 162-8640, Japan*

[d] *Department of Hematology, School of Medicine, Kitasato University, 1-15-1 Sagamihara, Kanagawa 228-8555, Japan*

[e] *Department of Pathology, National Institute of Infectious Diseases, 1-23-1 Toyama, Shinjuku-ku, Tokyo 162-8640, Japan*

[f] *Department of Applied Chemistry, Faculty of Science and Technology, Keio University, 3-14-1 Hiyoshi, Kohoku-ku, Yokohama, Kanagawa 223-0061, Japan*

Received 19 January 2008; accepted 9 April 2008
Available online 13 April 2008

Abstract

Epstein–Barr virus (EBV) causes EBV-associated lymphoproliferative diseases in patients with profound immune suppression. Most of these diseases are life-threatening and the prognosis of AIDS-associated lymphomas is extremely unfavorable. Polyclonal expansion of virus infected B-cell predisposes them to transformation. We investigated the possibility of nuclear factor kappa B (NF-κB) inhibition by dehydroxymethylepoxyquinomicin (DHMEQ) for the treatment and prevention of EBV-associated lymphoproliferative diseases. We examined the effect of DHMEQ on apoptosis induction in four EBV-transformed lymphoblastoid cell lines as well as peripheral blood mononuclear cells infected with EBV under immunosuppressed condition. DHMEQ inhibits NF-κB activation in EBV-transformed lymphoblastoid cell lines and induces apoptosis by activation of mitochondrial and membranous pathways. Using an *in vivo* NOD/SCIDγc mouse model, we showed that DHMEQ has a potent inhibitory effect on the growth of lymphoblastoid cells. In addition, DHMEQ selectively purges EBV-infected cells expressing latent membrane protein (LMP) 1 from peripheral blood mononuclear cells and inhibits the outgrowth of lymphoblastoid cells. These results suggest that NF-κB is a molecular target for the treatment and prevention of EBV-associated lymphoproliferative diseases. As a potent NF-κB inhibitor, DHMEQ is a potential compound for applying this strategy in clinical medicine.

Keywords: Epstein–Barr virus infections; NF-κB; DHMEQ

1. Introduction

Epstein–Barr virus (EBV) is a member of the γ-herpesvirus family that infects more than 90% of the world population and initially establishes latency III infection in B lymphocytes [1]. Latency III infection is characterized by the expression of the entire array of EBV latency genes, including EBV nuclear proteins (EBNA1, -2, -3A, -3B, -3C, and -LP), integral latent membrane proteins (LMP1, -2A, and -2B), the BamA

* Corresponding author. Tel.: +81 42 778 8111; fax: +81 42 778 8441.
** Tel.: +81 3 5803 5178; fax: +81 3 5803 0124.
*** Tel.: +81 3 5449 5298; fax: +81 3 5449 5418.
E-mail addresses: yamamoto.mmb@tmd.ac.jp (N. Yamamoto), tnabe@ims.u-tokyo.ac.jp (T. Watanabe), rhorie@med.kitasato-u.ac.jp (R. Horie).
[1] These authors contributed equally to this work.

1286-4579/$ - see front matter © 2008 Elsevier Masson SAS. All rights reserved.
doi:10.1016/j.micinf.2008.04.002